C830-L-02 NASI.29/3-2:00-11

NASA TechBriefs

National Aeronautics and Space Administration

Electronic Components and Circuits

Electronic Systems

Physical Sciences

Materials

Computer Programs

Mechanics

Machinery

Fabrication Technology

Hm 2002 004137

Mathematics and Information Sciences

Life Sciences

INTRODUCTION

Tech Briefs are short announcements of innovations originating from research and development activities of the National Aeronautics and Space Administration. They emphasize information considered likely to be transferable across industrial, regional, or disciplinary lines and are issued to encourage commercial application.

Availability of NASA Tech Briefs and TSPs

Requests for individual Tech Briefs or for Technical Support Packages (TSPs) announced herein should be addressed to

National Technology Transfer Center
Telephone No. **(800) 678-6882** or via World Wide Web at **www2.nttc.edu/leads/**

Please reference the control numbers appearing at the end of each Tech Brief. Information on NASA's Commercial Technology Team, its documents, and services is also available at the same facility or on the World Wide Web at **www.nctn.hq.nasa.gov**.

Commercial Technology Offices and Patent Counsels are located at NASA field centers to provide technology-transfer access to industrial users. Inquiries can be made by contacting NASA field centers and program offices listed below.

NASA Field Centers and Program Offices

Ames Research Center
Carolina Blake
(650) 604-1754 or
cblake@mail.arc.nasa.gov

Dryden Flight Research Center
Jenny Baer-Riedhart
(661) 276-3689 or
jenny.baer-riedhart@dfrc.nasa.gov

Goddard Space Flight Center
George Alcorn
(301) 286-5810 or
galcorn@gsfc.nasa.gov

Jet Propulsion Laboratory
Merle McKenzie
(818) 354-2577 or
merle.mckenzie@jpl.nasa.gov

Johnson Space Center
Hank Davis
(281) 483-0474 or
henry.l.davis1@jsc.nasa.gov

John F. Kennedy Space Center
Jim Aliberti
(321) 867-6224 or
Jim.Aliberti-1@ksc.nasa.gov

Langley Research Center
Sam Morello
(757) 864-6005 or
s.a.morello@larc.nasa.gov

Glenn Research Center
Larry Viterna
(216) 433-3484 or
cto@grc.nasa.gov

George C. Marshall Space Flight Center
Sally Little
(256) 544-4266 or
sally.little@msfc.nasa.gov

John C. Stennis Space Center
Kirk Sharp
(228) 688-1929 or
technology@ssc.nasa.gov

NASA Program Offices
At NASA Headquarters there are seven major program offices that develop and oversee technology projects of potential interest to industry:

Carl Ray
Small Business Innovation Research Program (SBIR) & Small Business Technology Transfer Program (STTR)
(202) 358-4652 or
cray@mail.hq.nasa.gov

Dr. Robert Norwood
Office of Commercial Technology (Code RW)
(202) 358-2320 or
rnorwood@mail.hq.nasa.gov

John Mankins
Office of Space Flight (Code MP)
(202) 358-4659 or
jmankins@mail.hq.nasa.gov

Terry Hertz
Office of Aero-Space Technology (Code RS)
(202) 358-4636 or
thertz@mail.hq.nasa.gov

Glen Mucklow
Office of Space Sciences (Code SM)
(202) 358-2235 or
gmucklow@mail.hq.nasa.gov

Roger Crouch
Office of Microgravity Science Applications (Code U)
(202) 358-0689 or
rcrouch@hq.nasa.gov

Granville Paules
Office of Mission to Planet Earth (Code Y)
(202) 358-0706 or
gpaules@mtpe.hq.nasa.gov

NASA Tech Briefs

National Aeronautics and Space Administration

November 2000
00-11

5 Electronic Components and Circuits

13 Electronic Systems

17 Physical Sciences

33 Materials

39 Computer Programs

45 Mechanics

49 Machinery

53 Mathematics and Information Sciences

This document was prepared under the sponsorship of the National Aeronautics and Space Administration. Neither the United States Government nor any person acting on behalf of the United States Government assumes any liability resulting from the use of the information contained in this document, or warrants that such use will be free from privately owned rights.

4

BLANK PAGE

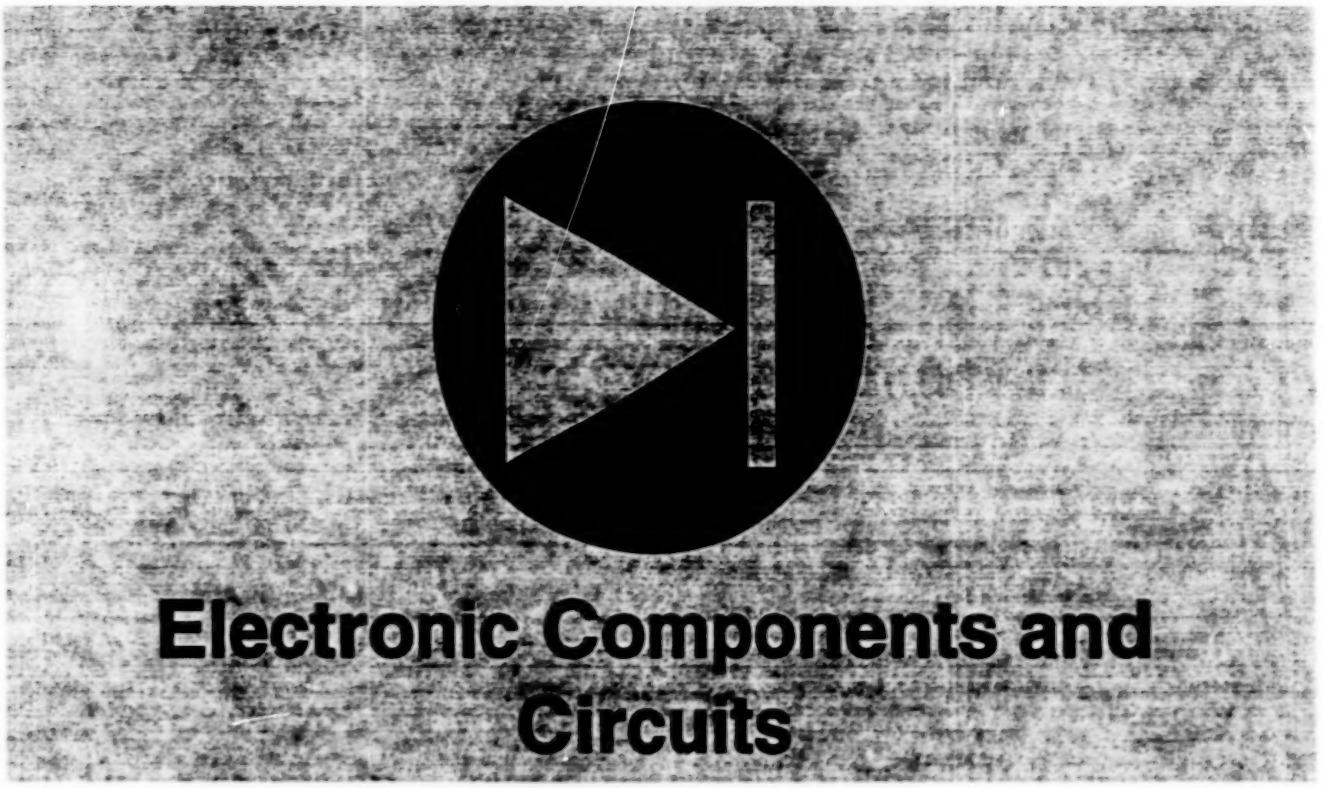

Electronic Components and Circuits

Hardware, Techniques, and Processes

7 Imager With Motion-Artifact Suppression and Antiblooming

8 Photodiode-Based CMOS APSs With Zero-Lag, Low-Noise, High-Linearity Design

9 Electrically Isolating, Thermally Coupling Devices

10 Improved Ignitor and Keeper Power Supplies for Hall Thruster

BLANK PAGE

Imager With Motion-Artifact Suppression and Antiblooming

This device operates in a snapshot mode, and residual charges are drained.

NASA's Jet Propulsion Laboratory, Pasadena, California

An improved photodiode-based complementary metal oxide/semiconductor (CMOS) active-pixel sensor (APS) incorporates features to (1) allow imaging with very high electronic shutter speeds, (2) suppress motion artifacts, and (3) prevent image lag and blooming (the spread of image lag to the area adjacent to a brightly illuminated area).

- Motion artifacts are distortions caused by motion in the scene imaged on a sensor. Ordinarily, a CMOS imager of older design is operated in a rolling-shutter mode, in which each row of pixels is exposed at a different instant of time. The rolling-shutter mode introduces distortion into the image; for example, if the scene contains an object moving in the direction of the

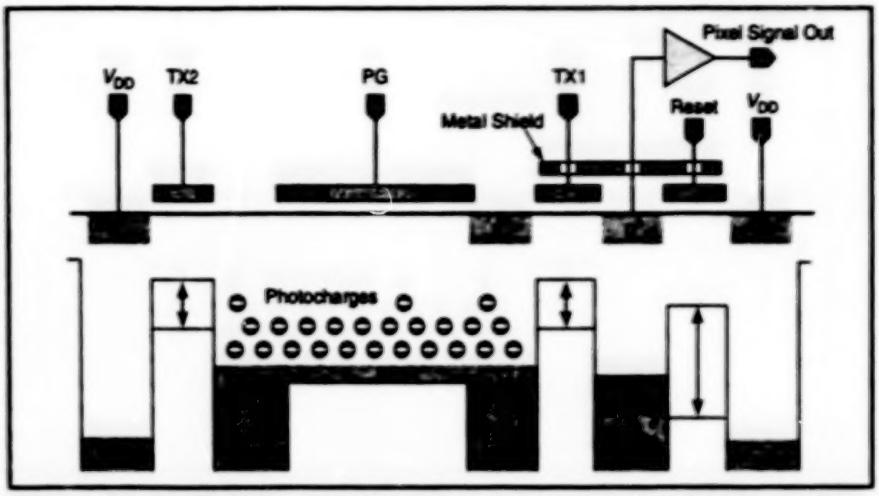

Figure 1. Two Transfer Gates and a Photogate are used to control the integration and detection of photocharges. TX2 acts as a lateral overflow gate and is used to drain residual charges between exposures to prevent image lag.

DEMONSTRATION OF SUPPRESSION OF MOTION ARTIFACTS
DEMONSTRATION OF SUPPRESSION OF IMAGE LAG
DEMONSTRATION OF SUPPRESSION OF BLOOMING
Rotating Fan at 30-ms Exposure
Image From Illuminated Dollar Bill (First of Two Consecutive Frames)
Image From Dollar Bill With Laser Spot Illumination
Rotating Fan at 100-μs Exposure
Image From Dollar Bill in the Dark (Second of Two Consecutive Frames)

Figure 2. These Test Images made with the improved CMOS APS demonstrate its ability to suppress motion artifacts, image lag, and blooming.

row exposure sequence, then in the output image, the object appears elongated in the direction of motion.
- Image lag is caused by retention of partial pixel image charges from previous frames. Blooming interferes with efforts to perform high-contrast, low-light imaging.

In the improved CMOS APS, motion artifacts are suppressed by rapid electronic shuttering in a snapshot mode; all pixels are exposed simultaneously. Blooming and image lag are prevented by draining residual pixel photocharges between frames. These improvements are made possible by a unique design implemented in standard single-polysilicon CMOS.

Figure 1 is a schematic cross section of a single-pixel portion of the device. Photocharge is integrated under the photogate (PG). The integration (exposure) time is controlled by a voltage pulse applied to the PG; in general, the exposure time can be thus defined to within 10 μs in this and all other pixels.

There are two transfer gates: TX1 and TX2. The transfer gates are common to the entire CMOS APS chip and are operated by application of voltage pulses timed in conjunction with the voltage pulse applied to the PG. By virtue of fabrication in standard CMOS single-polysilicon CMOS, the gates are separated by floating n^+ diffusions. TX1 is used for transferring the integrated photocharge to a sensing node for detection. TX2 serves both as an antiblooming gate and for defining exposure time. The sensing node serves as part of a frame buffer, which makes it possible to perform frame readout at any time after charge integration, independently of the charge-integration time.

Although the exposure time is defined by the duration of the pulse applied to the PG, the floating diffusions continue to collect photocharges. The transfer of these residual photocharges to the sensing node is the cause of image lag in a CMOS APS of older design. In the present CMOS APS, these charges are drained off, prior to beginning integration of charge for the next frame, by application of voltage pulses with suitable timing and levels to the PG and TX2.

Figure 2 presents some test images acquired by use of the improved CMOS APS:
- Snapshots of a fan rotating at 1,800 revolutions per minute were made with 30-ms and 100-μs exposures. The 100-μs image demonstrates the ability of the device to "freeze" the motion of the fan without introducing motion artifacts.
- Images of George Washington on a dollar bill were made in two consecutive frames with illumination in during the first frame and darkness during the second one. No residual image was observed in the second frame.
- Another image of George Washington on a dollar bill was made with ordinary illumination plus spot illumination by a laser. No blooming was observed, even though the laser illumination was 80 dB above the saturation level of the device.

This work was done by Bedabrata Pain, Guang Yang, Orly Yadid-Pecht, and Chris J. Wrigley of Caltech for ***NASA's Jet Propulsion Laboratory****. Further information is contained in a TSP [see page 1].*

In accordance with Public Law 96-517, the contractor has elected to retain title to this invention. Inquiries concerning rights for its commercial use should be addressed to

Technology Reporting Office
JPL
Mail Stop 122-116
4800 Oak Grove Drive
Pasadena, CA 91109
(818) 354-2240

Refer to NPO-20555, volume and number of this NASA Tech Briefs *issue, and the page number.*

Photodiode-Based CMOS APSs With Zero-Lag, Low-Noise, High-Linearity Design

These image detectors offer the best of both "hard" and "soft" reset.

NASA's Jet Propulsion Laboratory, Pasadena, California

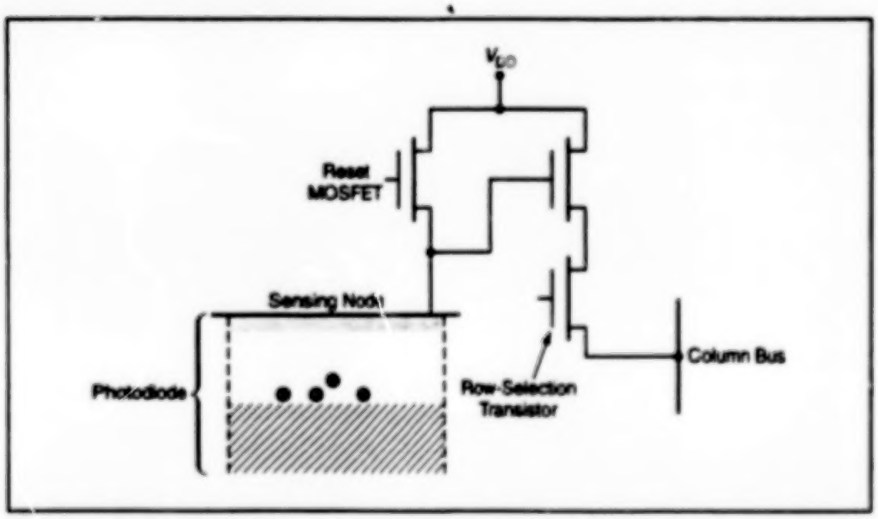

Figure 1. A Typical Prior CMOS APS Circuit is designed and operated according to a soft- or a hard-reset scheme. Both schemes entail advantages and disadvantages.

Two improved schemes for the design and operation of photodiode-based CMOS (complementary metal oxide/semiconductor) active-pixel sensors (APSs) afford zero image lag, low noise, and high linearity of response even under low illumination. Figure 1 schematically depicts the circuitry for one pixel according to a typical older scheme. In soft reset, the sensing node does not charge up to the power-supply potential (V_{DD}), and depends strongly on the potential at the beginning of the reset. In hard reset, the sensing node charges up to a known potential, usually V_{DD}.

For reasons that are complex and must therefore be omitted from this article for the sake of brevity, typical older soft- and hard-reset schemes entail disadvantages and advantages as follows:
- Soft reset advantageously results in low-noise output and a high power-supply rejection ratio (PSRR). However, disadvantageously, soft reset results in image lag of as much as 70 percent of the mean signal in the previous frame, and a markedly nonlinear response under low illumination.
- Hard reset advantageously eliminates image lag but disadvantageously results in increased read noise, dark current, and reduced power-supply ratio.

Under the improved schemes, the disadvantages are eliminated by resetting pixels first by hard reset and then by soft reset. Hard reset erases the memory from the

previous frame, eliminating image lag and nonlinearity, while soft reset allows operation with low-read noise. Thus, low noise, zero image lag, and high linearity are achieved simultaneously.

Figure 2 illustrates the pixel circuits that are used for implementation of the two new schemes, which are characterized by the terms "flushed photodiode" and "hard-to-soft (HTS) reset photodiode," respectively. In the flushed-photodiode APS, the pixel circuit contains an additional line (denoted "$\overline{\text{HTS}}$") for a row-decoded signal that controls the potential at the drain of the reset MOSFET (metal oxide/semiconductor field-effect transistor). Pulsing HTS reduces the drain potential, allowing the pixel to be reset in hard reset mode. In the HTS APS, no change in the pixel design is necessary. In this scheme, V_{DD} is routed to each column through an n- and a p-channel MOSFET. The gate of the p-channel MOSFET is connected to a line (denoted "HTS") that carries a column-decoded signal. Pulsing HTS momentarily high during the reset phase causes the source of the reset MOSFET to reduce below V_{DD}, causing the pixel to go into hard reset. The hard-reset level is determined by the size of the n-channel MOSFET, and is set to approximately $V_{DD}/2$. In both schemes, soft reset of the pixel following the hard reset is achieved once the HTS pulse goes low.

This work was done by Bedabrata Pain, Guang Yang, Thomas Cunningham, and Bruce Hancock of Caltech for **NASA's Jet Propulsion Laboratory**. *For further information, access the Technical Support Package (TSP)* ***free on-line at www.nasatech.com*** *under the category.*

In accordance with Public Law 96-517, the contractor has elected to retain title to this invention. Inquiries concerning rights for its commercial use should be addressed to

Technology Reporting Office
JPL
Mail Stop 122-116
4800 Oak Grove Drive
Pasadena, CA 91109
(818) 354-2240

Refer to NPO-20716, volume and number of this NASA Tech Briefs *issue, and the page number.*

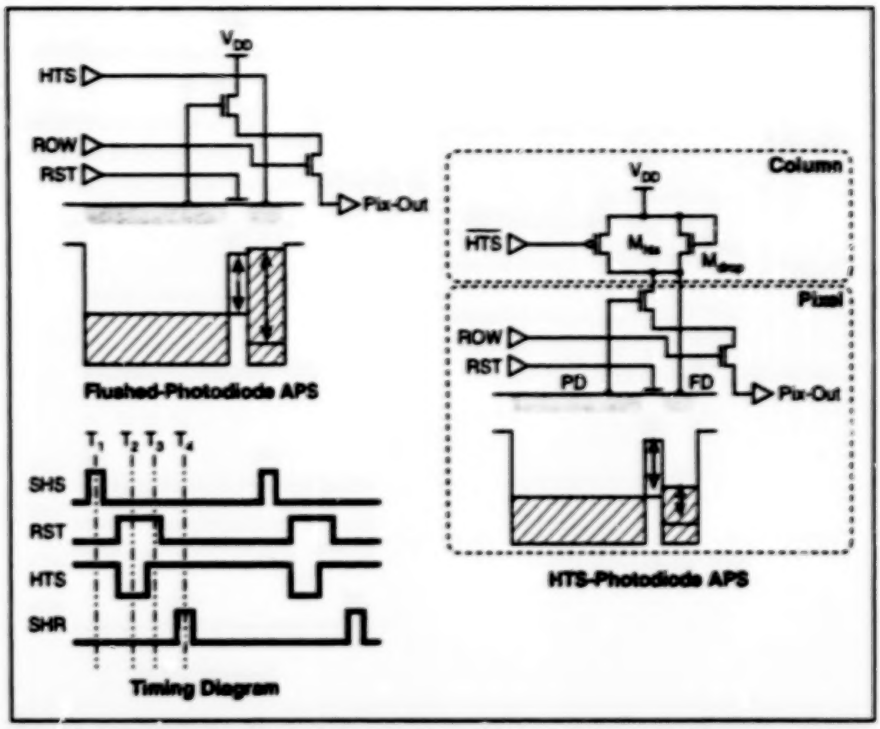

Figure 2. These Pixel Circuits are designed and operated to go into hard reset followed by soft reset.

Electrically Isolating, Thermally Coupling Devices

Digital signals would be coupled thermally instead of electrically or optically.

NASA's Jet Propulsion Laboratory, Pasadena, California

Integrated signaling devices of a proposed type would utilize thermal coupling to transfer digital signals between electronic circuits that are required to be kept electrically isolated from each other. The proposed devices would be implemented as silicon-on-insulator complementary metal oxide/semiconductor (SOI CMOS) integrated circuits and could therefore be readily integrated with other SOI CMOS devices. For some applications, the proposed devices could be an attractive alternative to conventional optocouplers, which have not been amenable to integration with CMOS devices because of a lack of silicon-based integrated sources of light.

The thermal-coupling concept offers a major advantage at the outset: There are several possible methods for on-chip conversion of electrical signals to thermal ones, and there already exists a significant body of published work on the conversion of thermal signals to electrical ones.

Though optimization of design can be expected to entail significant effort with attention to minute details, the basic principle of operation and design concept (see figure) are straightforward. The device would include an input circuit (e.g., an amplifier), through which an input digital signal pulse would be applied to a resistor to generate a pulse of heat. The thermal pulse would be conducted from the resistor, through an electrically insulating barrier, to a thermal sensor.

The resistive heater could be made of polycrystalline silicon. The thermally conducting, electrically insulating barrier would likely be made of a thin layer of SiO_2. A simple thermal lens could be made from a suitably patterned surface layer of aluminum. (A more complex thermal lens might also include micromachined, embedded metallic heat pipes to decrease the thermal-response time.) The thermal sensor could be a silicon p/n diode.

A possible disadvantage is that the characteristic times of thermal propagation of signals could limit the speed of such a device. The propagation delay, coupling efficiency, and degree of electrical isolation of the thermal-transducer portion of the device are related to a combination of several geometrical factors. For example, as the distance between the resistor and the thermal sensor increases, the speed and the coupling efficiency decrease. The shape of the lens also exerts a significant effect on the coupling efficiency and speed.

Another major concern is that of input power. High instantaneous input power would translate to a larger signal and faster input/output coupling, but there is also a

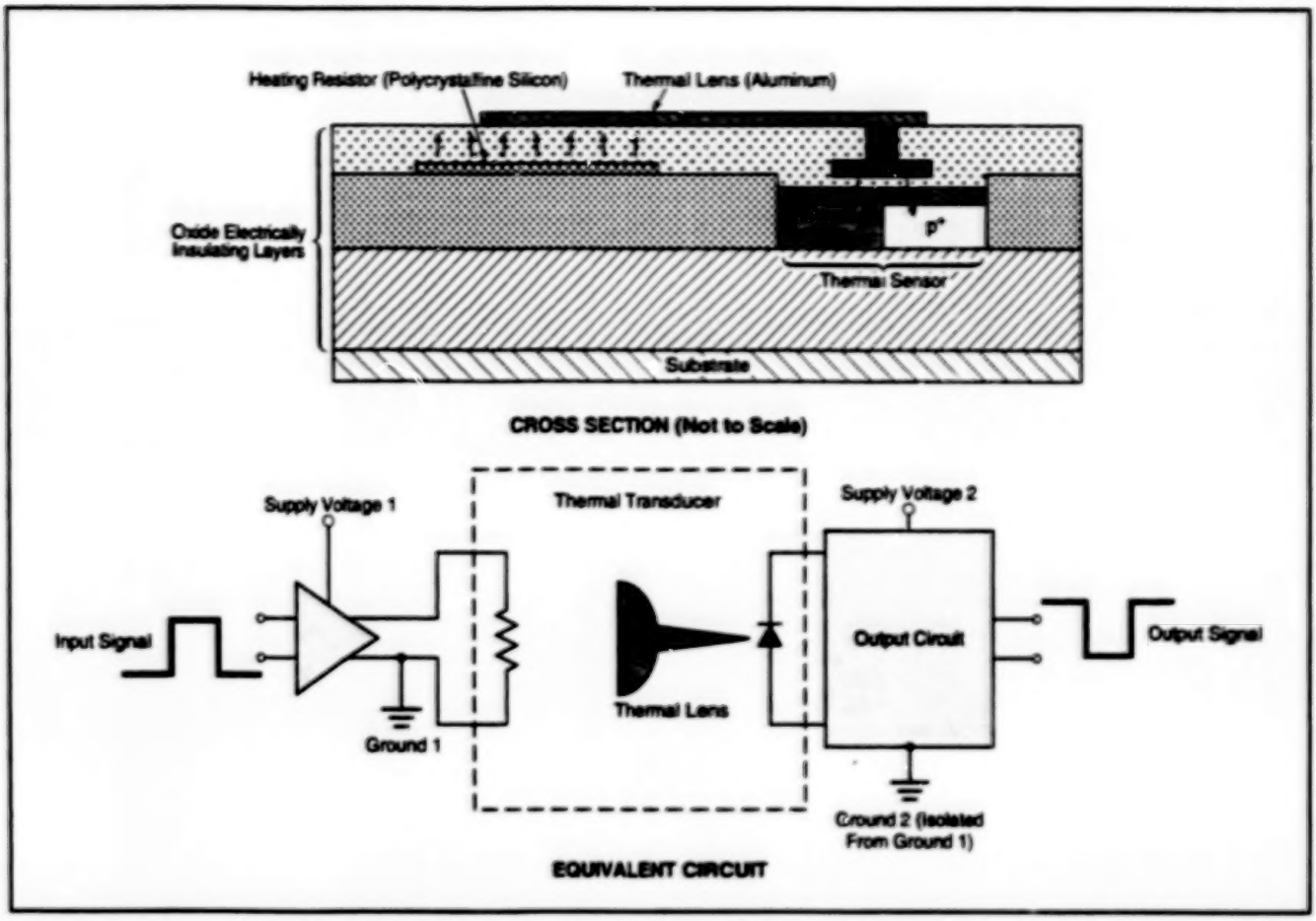

A Electrically Isolating, Thermally Coupling Device according to the proposal would be an SOI CMOS integrated circuit that would include an input electronic circuit, an electrically isolating thermal transducer, and an output electronic circuit.

need to conserve energy and minimize spurious heating. A smarter alternative would be to design an input driver circuit that would produce (1) a shorter higher-power electrical pulse to generate a rapidly rising thermal pulse, followed by (2) a longer, lower-power pulse for maintaining the thermal pulse. The higher-power initial input pulse would thus ensure the rapid triggering of the output circuit via the thermal sensor, and the subsequent longer, lower-power input pulse would guarantee the triggered state of the output circuit. The combination of the two power pulses would result in less power demand than would the use of simple high-power pulses. It would be necessary to select an optimal combination of power levels and pulse durations as a compromise between minimizing average power consumption and maintaining the integrity of signals.

A third major concern is that the thermal signal would include a varying ambient-temperature component. It would be necessary to design the output circuit to reject this component and rapidly convert the rest into an equivalent electrical signal. Two key parameters for designing this circuit are the resolution of the thermal detector and its conversion speed. It may be necessary to amplify the output of the thermal sensor and feed the amplified signal as input to an output driver with digital hysteresis.

This work was done by Mohammad Mojarradi of Caltech for **NASA's Jet Propulsion Laboratory**. *Further information is contained in a TSP [see page 1].*

In accordance with Public Law 96-517, the contractor has elected to retain title to this invention. Inquiries concerning rights for its commercial use should be addressed to

Technology Reporting Office
JPL
Mail Stop 122-116
4800 Oak Grove Drive
Pasadena, CA 91109
(818) 354-2240

Refer to NPO-20640, volume and number of this NASA Tech Briefs *issue, and the page number.*

Improved Ignitor and Keeper Power Supplies for Hall Thruster

The key to reliable operation of a cold cathode is correct power-supply waveforms.

John H. Glenn Research Center, Cleveland, Ohio

Ignitor and keeper power supplies have been developed specifically for a Hall-effect thruster with a cold cathode. Prior to the development of these power supplies, difficulties had been observed in the operation of cold-cathode Hall thrusters; in particular, they did not start reliably upon turn-on of power. Many specialists in Hall thrusters had attributed the difficulties to the characteristics of cold cathodes as distinguished from those of hot cathodes.

The development of the present ignitor and keeper power supplies was guided by the observation that the key to reliable operation of cold-cathode Hall thrusters is to use

correct power-supply waveforms and that the unreliability of startup observed previously was caused by the use of incorrect waveforms. The present power supplies comprise (1) an igniter supply that produces a clean 1,000-V pulse with no undershoot and (2) a current-limited keeper supply. The combination of these power supplies produces a waveform that can be relied upon to start operation of a cold cathode on a stationary plasma thruster. The waveform produced by these power supplies can also be used to clean a cathode that has been contaminated by exposure to the environment.

This work was done by See-pok Wong, E. "Ned" J. Britt, and Raymond Lin of Space Power, Inc., **Glenn Research Center**.

Inquiries concerning rights for the commercial use of this invention should be addressed to NASA Glenn Research Center, Commercial Technology Office, Attn: Steve Fedor, Mail Stop 4–8, 21000 Brookpark Road, Cleveland, Ohio 44135. Refer to LEW-16490.

BLANK PAGE

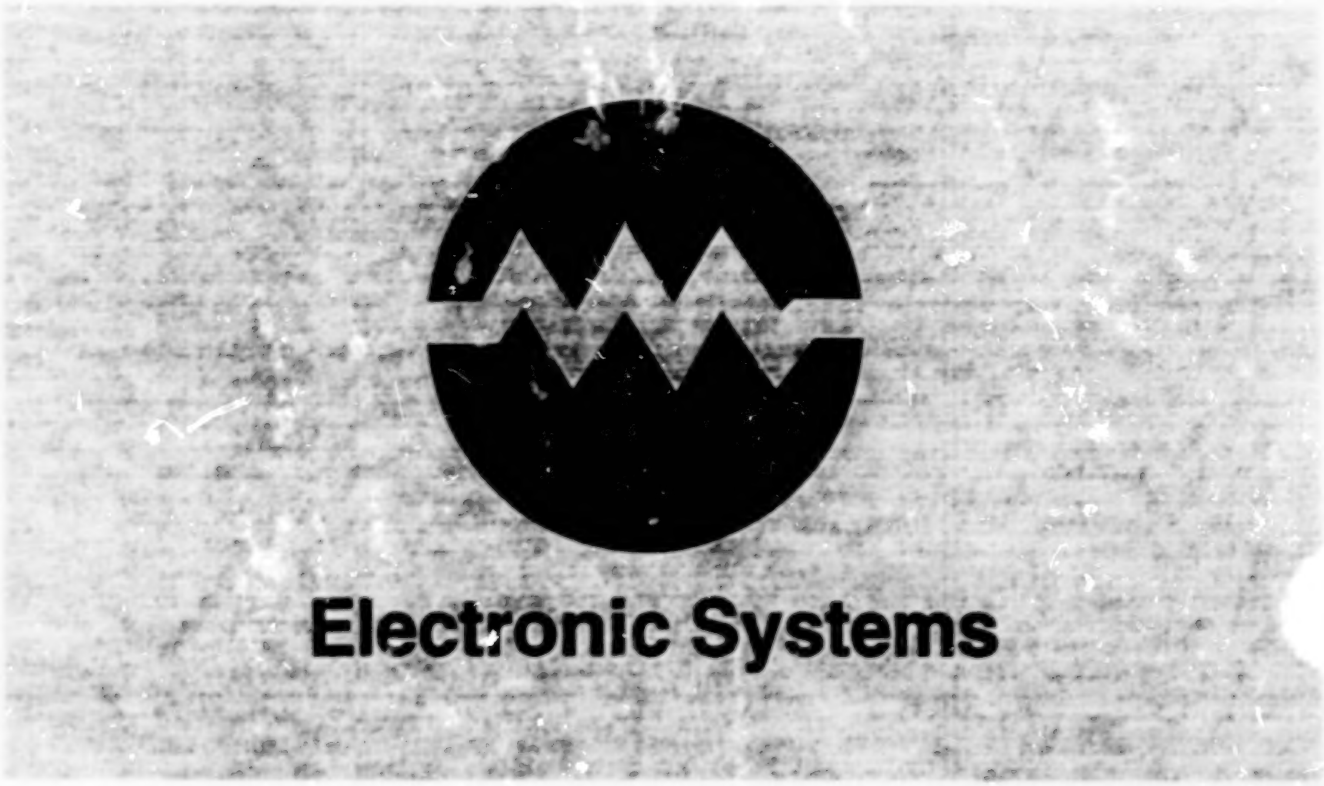

Hardware, Techniques, and Processes

15 Frequency-Converting Photonic Link With BSSA Amplification

14

BLANK PAGE

Frequency-Converting Photonic Link With BSSA Amplification

Undesired polarization and dispersion effects are suppressed.

NASA's Jet Propulsion Laboratory, Pasadena, California

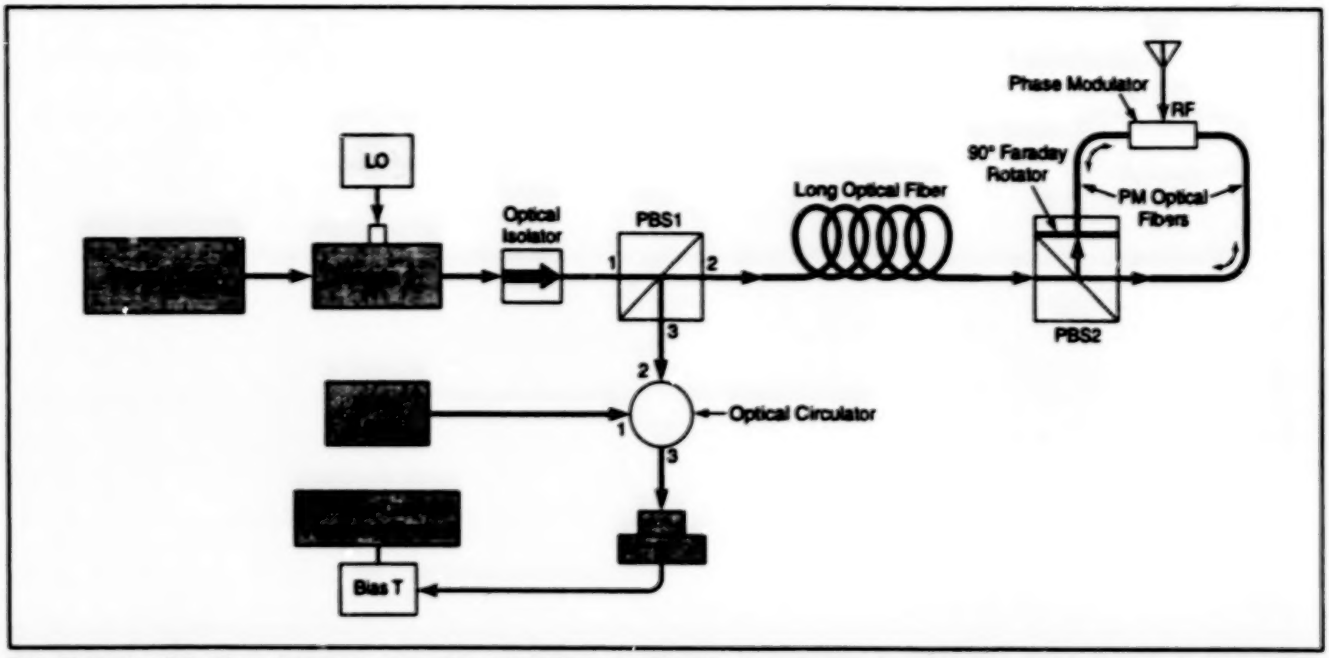

This Photonic Link effects frequency conversion and Brillouin amplification, is insensitive to polarization, and is immune to signal fading caused by dispersion.

A photonic system has been devised for acquiring a radio-frequency (RF) signal from a remote receiving antenna via a long optical fiber. The system performs multiple functions, including upward or downward frequency conversion, optical amplification [more specifically, Brillouin selective sideband amplification (BSSA)] in the long optical fiber, and other functions, the combined effects of which are to eliminate sensitivity to polarization and to minimize signal fading caused by dispersion in the long optical fiber. The basic design of the system also makes it possible to use phase modulators. In comparison with amplitude modulators, phase modulators exhibit lower losses and cost less; moreover, unlike amplitude modulators, phase modulators do not require bias and thus do not present any bias-stabilization problems in design and operation.

The system (see figure) includes a signal laser, which generates an optical carrier signal. An electronic or optoelectronic local oscillator (LO) generates a stable and spectrally pure RF subcarrier signal (typically at a frequency of 10 GHz) for use in frequency conversion. This subcarrier signal is used to modulate the optical carrier signal. (Phase modulation is preferable to amplitude modulation for the reasons stated above.) The modulated optical signal is then injected, via an optical isolator and a first polarizing beam splitter (PBS1), into the long optical fiber for propagation to the remote antenna site. This is a standard single-mode optical fiber and is typically several kilometers long.

After propagation to the remote antenna site, the polarization of the modulated carrier signal is no longer linear, and it varies when the fiber is disturbed. A second polarizing beam splitter (PBS2) separates the two polarization components, and the polarization of one of these components is modified by a 90° Faraday rotator that is incorporated into PBS2. Polarization-maintaining (PM) optical fibers are used to connect the two output ports of PBS2 to opposite ends of a phase modulator, to which the RF signal from the antenna is applied. The slow axis of each PM fiber is aligned with the polarization of the PBS2 port to which it is connected. As a result of this arrangement, the two polarization components are converted to two oppositely travelling, identically polarized light beams in the phase modulator. These beams are modulated equally by the RF signal. After passing through the phase modulator, these beams are recombined by PBS2 and sent back along the long optical fiber. The net effect of this ring- arrangement/polarization-conversion/modulation scheme is to eliminate sensitivity of the modulator to polarizing effects in the long optical fiber.

Because of the 90° Faraday rotator in the modulator ring, at every location along the long optical fiber, the light propagating backward (away from the antenna) is polarized orthogonally to the light propagating forward (toward the antenna). The backward-propagating beam is separated in PBS1 and is coupled via an optical circulator to a photodetector. The photodetector is connected to a bias T, which separates the RF, LO, and intermediate-frequency (IF) components of the photocurrent. One of these frequency components is selected and is used as a feedback control signal to lock the frequency of the pump laser to a desired modulation sideband of the signal laser, as described in the paragraph after next.

A pump laser generates a beam of light needed for BSSA. The pump beam is coupled, via the optical circulator, into port 3 of PBS1. The polarization of the pump beam is so adjusted that the pump beam leaves PBS1 through its port 2 and propagates forward along the long optical fiber. After passing through the PBS2/modulator ring, the pump beam propagates back along the long optical fiber and enters port 2 of PBS1. Because of the action of the PBS2/modulator ring, the polarization state of the backward-going pump beam is orthogonal to that of the forward-going

pump beam everywhere along the fiber. The polarization state of the forward-going pump beam is also everywhere the same as that of the backward-going modulated signal beam; this condition is optimum for Brillouin amplification everywhere along the fiber and eliminates the sensitivity of the Brillouin amplification to polarization. The pump beam leaves through port 1 of PBS1 and is attenuated by the optical isolator.

By tuning the frequency of the pump laser, one can make the narrow frequency-shift (Stokes-frequency) band associated with the Brillouin backscattering of the pump laser light to overlap one of the phase-modulation sidebands of the signal beam, thereby enabling Brillouin amplification of that sideband. The amplification of this modulation sideband breaks the perfect amplitude balance of sidebands of phase modulation and thereby converts the phase modulation to amplitude modulation. One can amplify either an LO or an RF sideband to obtain amplified IF and RF signals at the receiver. When the LO sideband is chosen, the beats of the amplified LO sideband with the upper and lower RF sidebands in the photodetector produce a down-converted and an up-converted IF signal, while the beat between the amplified LO sideband and the signal carrier produces an amplified LO signal.

This work was done by X. Steve Yao of Caltech for **NASA's Jet Propulsion Laboratory**. *Further information is contained in a TSP [see page 1].*

In accordance with Public Law 96-517, the contractor has elected to retain title to this invention. Inquiries concerning rights for its commercial use should be addressed to

Technology Reporting Office
JPL
Mail Stop 249-103
4800 Oak Grove Drive
Pasadena, CA 91109
(818) 354-2240

Refer to NPO-20759, volume and number of this NASA Tech Briefs *issue, and the page number.*

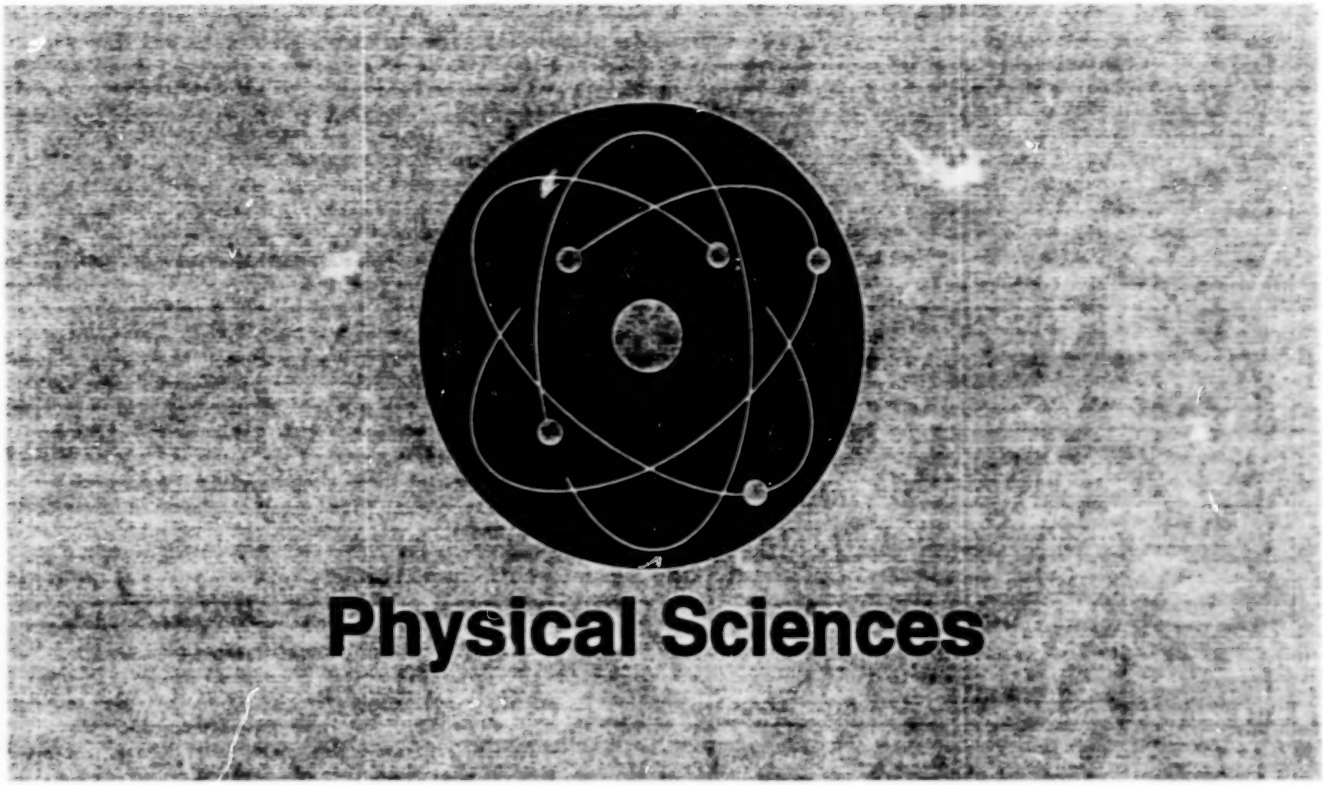

Physical Sciences

Hardware, Techniques, and Processes

19 Magnetically Enhanced Propellant Isolator for Ion Sources
20 Passive Radiative Cooler for Use in Outer Space
21 Helium Leak Detector With Improved Sample-Delivery System
22 Liquid Shell Insulation
23 Fluorometer for Analysis of Photosynthesis in Phytoplankton
24 Improved Illumination Device for Inspecting Window Surfaces
25 Gas Analyzer Measures Concentrations of H_2, O_2, and H_2O
26 Phonon-Assisted Quantum-Well Infrared Photodetector
27 Coupling Light Between Optical Fibers and Noncircular Beams
28 Fast Infrared Spectrometer
29 Whispering-Gallery-Mode Microspheres as Light Modulators
30 Magnetostrictive Heat Switches Actuated by Flux Tubes
30 Magnetostrictive Valves Actuated by Flux Tubes
31 Fiber-Optic Sensors for Measuring Oxygen Dissolved in Water
31 Buoy Instrumented for Spectral Measurement of Water Quality

BLANK PAGE

Magnetically Enhanced Propellant Isolator for Ion Sources

A magnetic field inhibits the diffusion of electrons.

John H. Glenn Research Center, Cleveland, Ohio

A magnetically enhanced, high-voltage propellant isolator has been conceived for incorporation into materials-processing or space-based ion systems. The high-voltage isolator is needed to provide electrical isolation between the ion source, typically at high voltage, and the gas-feed system.

Heretofore, it has been the usual practice to provide the required electrical isolation by installing ceramic breaks (section of ceramic tubes) between grounded gas-feed lines and the high-voltage plasma source, as shown in the upper part of Figure 1. Unfortunately, at operating pressures between 13 Pa and 13 kPa and kilovolt potentials, the short ceramic spacer can often fail due to electrical breakdown of the feed gas, thereby causing a highly conductive plasma discharge to form inside the ceramic. Such breakdowns effectively short the ion source to near ground potentials, thus preventing high-voltage operation.

A magnetically enhanced, high-voltage isolator, as shown in the lower part of Figure 1, consists of a conventional ceramic isolator immersed in a strong transverse magnetic field. The strong, transverse field is provided by commercially available rare-earth magnets. The magnetic field increases the breakdown voltage at a given isolator internal pressure, thereby widening the range of operating conditions over which breakdown does not occur.

The primary purpose of the magnetic field is to severely restrict the motion of electrons parallel to the axis of the isolator. To first approximation, electrons are constrained to move in circles about magnetic-field lines and can diffuse across the transverse field only by collision with neutral molecules or ions. To inhibit the diffusion of electrons along the axis so as to prevent avalanche formation and breakdown, the magnetic field must be strong enough such that the electron cyclotron frequency (which is proportional to the magnetic-field strength) greatly exceeds the frequency of collisions between electrons and neutrals.

A prototype magnetically enhanced isolator was constructed by placing rare-earth magnets on opposite sides of a conventional isolator. The transverse magnetic field associated with this configuration was 2.6 kG on centerline. In tests at various gas pressures, the breakdown potential of the magnetically-enhanced isolator were found to exceed those of the same isolator without magnetic enhancement (see Figure 2). The greatest increase in breakdown potential was achieved at low pressures; this was expected because under those conditions, electron motion is sufficiently magnetized due to the lower electron-neutral collision frequency.

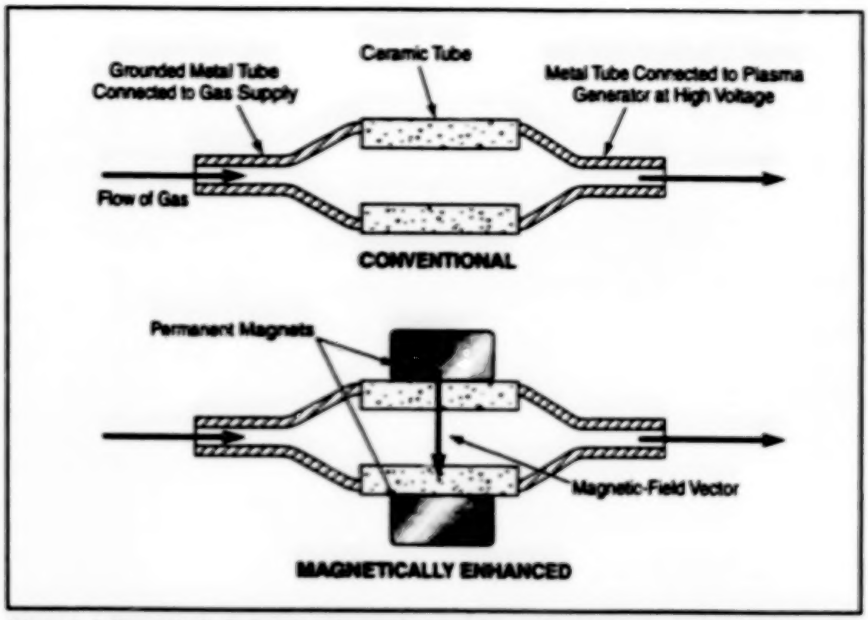

Figure 1. A Magnetically Enhanced Propellant Isolator, which isolates the gas-feed line from the ion source, is basically a conventional isolator tube sandwiched between permanent magnets that generate a strong, transverse field.

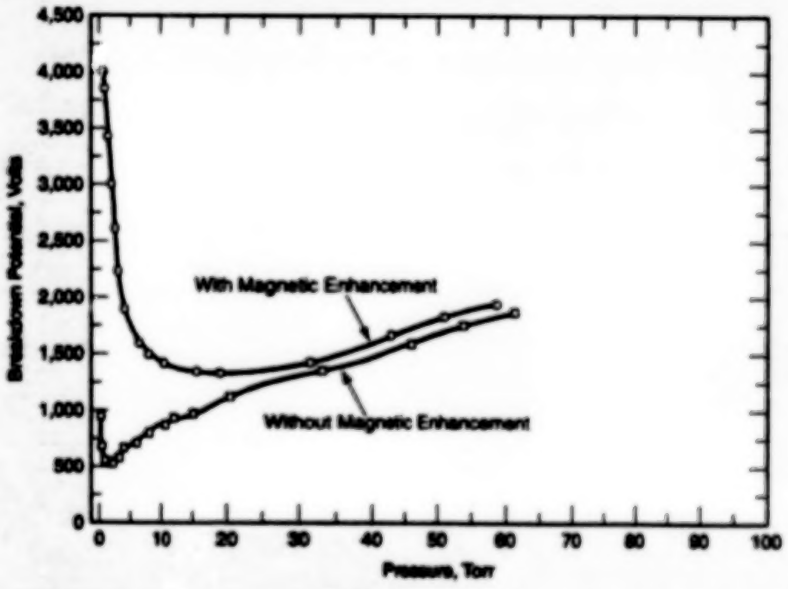

Figure 2. The Breakdown Potential applied between the ends of a prototype isolator tube similar to that of Figure 1, with and without magnetic enhancement, was measured as a function of xenon gas pressure. These plots have the form of typical Paschen breakdown curves.

This work was done by John E. Foster of **Glenn Research Center**. *Further information is contained in a TSP [see page 1].*

Inquiries concerning rights for the commercial use of this invention should be addressed to NASA Glenn Research Center, Commercial Technology Office, Attn: Steve Fedor, Mail Stop 4–8, 21000 Brookpark Road, Cleveland, Ohio 44135. Refer to LEW-16749.

Passive Radiative Cooler for Use in Outer Space

High-temperature superconductors are cooled radiatively to operating temperatures.

Lyndon B. Johnson Space Center, Houston, Texas

The figure depicts a passive radiative cooler designed for use in outer space. The design of this device conjoins radiative and conductive thermal-isolation features, which, in further conjunction with a favorable spacecraft attitude and on-orbit thermal environment, can be utilized to cool specimens of high-temperature superconducting materials to operating temperatures. Once installed on a spacecraft or even on the lunar surface, the passive radiative cooler will perform the cooling function that would otherwise be performed by a more expendables-hungry cryogenic system. This device, which has the added advantage of no moving parts, can operate in low orbit around the Earth in the space-shuttle cargo bay. Small and adaptable to many spacecraft and mounting configurations, this device can be used to demonstrate applications that involve superconductivity. Commercially, this device can advance the art by providing a simplified alternative for satellites equipped with infrared (IR) detectors or apparatuses that exploit superconductivity.

The current art in cooling sensors or specimens of superconducting or other materials in outer space involves the use of cryogenic cooling systems; the operation of such systems is more complex and certainly more costly in expendables (cryogenic fluids) than is the use of the passive radiative cooling capability of outer space itself. Though radiative coolers other than the present one have been used before in outer space, those devices can operate only on interplanetary spacecraft, on spacecraft in high orbit around the Earth, or on spacecraft in low orbit around the Earth under tailored illumination conditions (i.e., Sun-synchronous orbits). The thermal-radiation environment of a high orbit around the Earth differs markedly from that of a low orbit around the Earth: the proximity of the Earth gives rise to undesirable heating by IR radiation from the Earth plus reflected solar radiation reflected from the Earth (albedo) from a large portion of the field of view. The present passive radiative cooler provides shielding against the radiation from the Sun and Earth and is of a size and simplicity that make it suitable for operation in the space-shuttle cargo bay, which is also a source of IR heating.

The three main components of the passive radiative cooler are a mounting base, a conical shade, and a conical radiator/sample tray. The mounting base includes a low-thermal-conductance structure for holding the conical shade. The conical radiator is suspended within the conical shade by tensioned nonmetallic cords, which provide (1) a high degree of isolation against thermal conduction and (2) protection against vibration for the sample tray and the radiator. Both the outside of the conical radiator and the inside of the conical shade are fabricated with a low-IR-emittance finish for a high degree of radiative isolation. The inside of the conical radiator is given a high-IR-emittance finish to promote high radiative transfer of heat to space.

An item that one seeks to cool (e.g., a specimen of a high-temperature superconductor) is affixed to the sample tray, and the passive radiative cooler is mounted on a

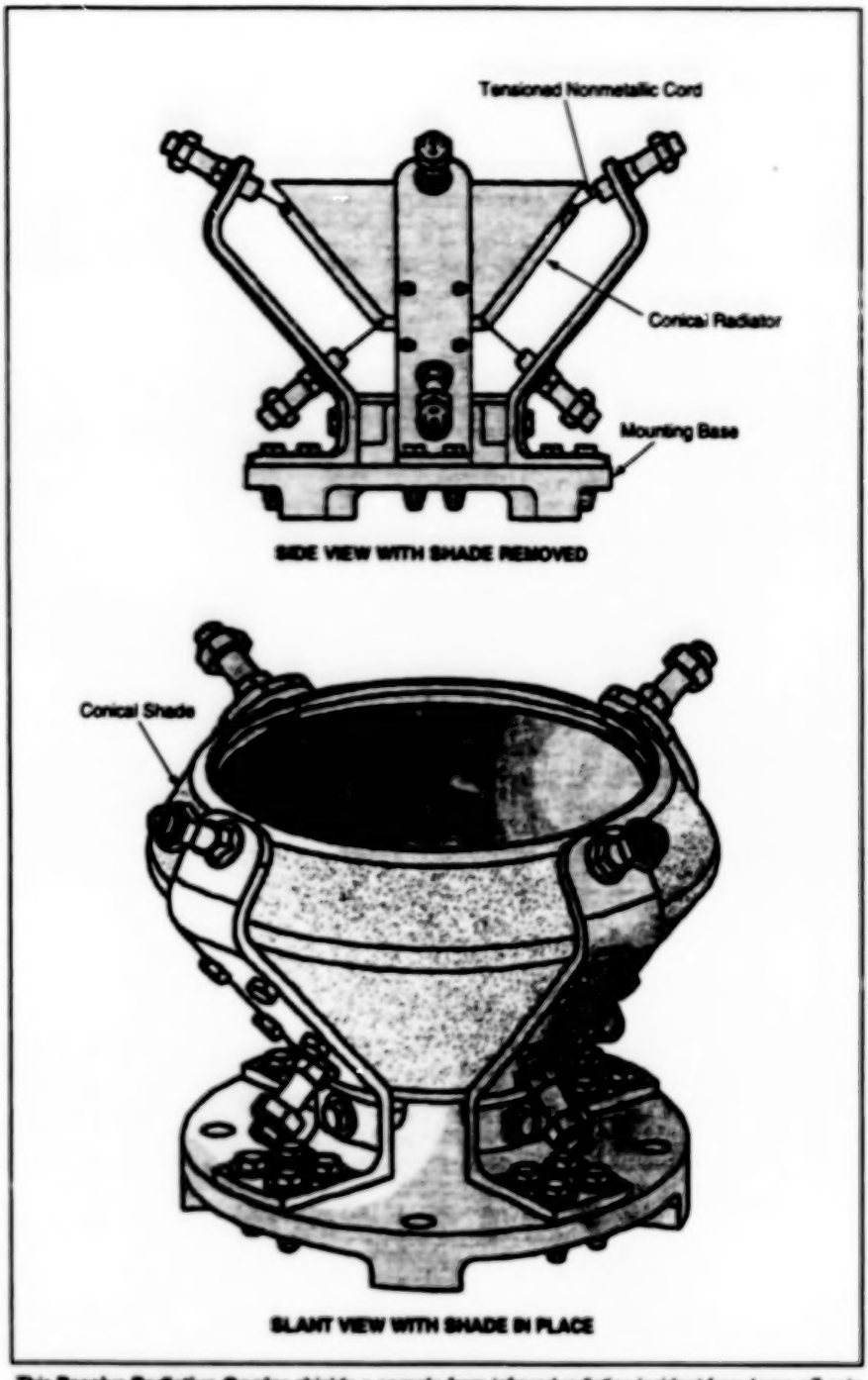

This Passive Radiative Cooler shields a sample from infrared radiation incident from large off-axis angles while allowing infrared radiation to escape to space at angles closer to the axis.

spacecraft structure that faces away from the Sun or a planet. As the spacecraft orbits in a specified attitude, the sample tray and sample are cooled radiatively. The cone angle of the radiator is chosen to afford adequate radiative heat rejection while enabling the cone to shield the sample from viewing other bodies (the Earth, the Sun, or nearby objects) that could adversely affect heat balance of the sample.

A relatively high degree of thermal isolation can be achieved. For example, in a test of a prototype of the passive radiative cooler, a sample temperature of 116 K was achieved in the presence of a mounting surface at a temperature of 240 K.

The passive radiative cooler is expected to function within a remarkable temperature range. The basic passive-radiative-cooler design is flexible and scalable; for example, if the device is to be mounted in a location with few nearby obstructions, it could be beneficial to design for a more open cone. The passive radiative cooler can be mounted on a spacecraft for cooling samples of high-temperature superconductors or other materials, detectors, or sensors, provided the environment and spacecraft attitude meet the specified criteria. Finally, again assuming that sufficient isolation from the surface can be achieved, the passive radiative cooler can even be used on the lunar surface to cool sensors.

This work was done by Steven L. Rickman, Ross G. Iacomini, David S. McCann, Robert G. Brown, and Yuan-Chyau Chang of **Johnson Space Center** *and by Jeffrey A. Clayhold, Ching-Wu (Paul) Chu, Allen W. Linnen, Jr., and Yuyi Xue of the Texas Center for Superconductivity, University of Houston.*
MSC-22712

Helium Leak Detector With Improved Sample-Delivery System

The pressure at the inlet of a mass spectrometer is regulated.

John F. Kennedy Space Center, Florida

The figure schematically depicts a portable helium leak detector that includes an improved sample-delivery system. This instrumentation is designed for detecting leaks in the fuel and oxidizer systems of the space shuttle main engines. In a helium leak test, helium is used as a tracer gas in place of the hazardous fuel or oxidizer. The fuel or oxidizer plumbing of interest is pressurized with helium. The aft section of the space shuttle (which section contains the plumbing) is purged with air, and the portable helium leak detector is used to monitor for any increase in helium content of the purge exhaust at concentrations down to the part-per-million level. The portable helium leak detector can also be used to perform tests to detect very small leaks in systems other than the space shuttle main engines.

The portable helium leak detector includes three instrumentation modules: a commercial helium leak detector, a control system, and a sample-delivery system. These modules, plus gas supplies, are mounted on one cart that can be wheeled to the test location.

Like other commercial helium leak detectors, the present one is essentially a mass spectrometer designed specifically for detecting helium. The inlet of the mass spectrometer is attached to the outlet of the sample-delivery system. The mass spectrometer is connected to the control system via an RS-232 serial data port.

The control system includes a laptop computer connected via serial data ports to solid-state relays and analog-to-digital converters that, in turn, are connected to the mass spectrometer and the sample-delivery system. The computer runs LabView software that controls the general sequencing of events, the switching

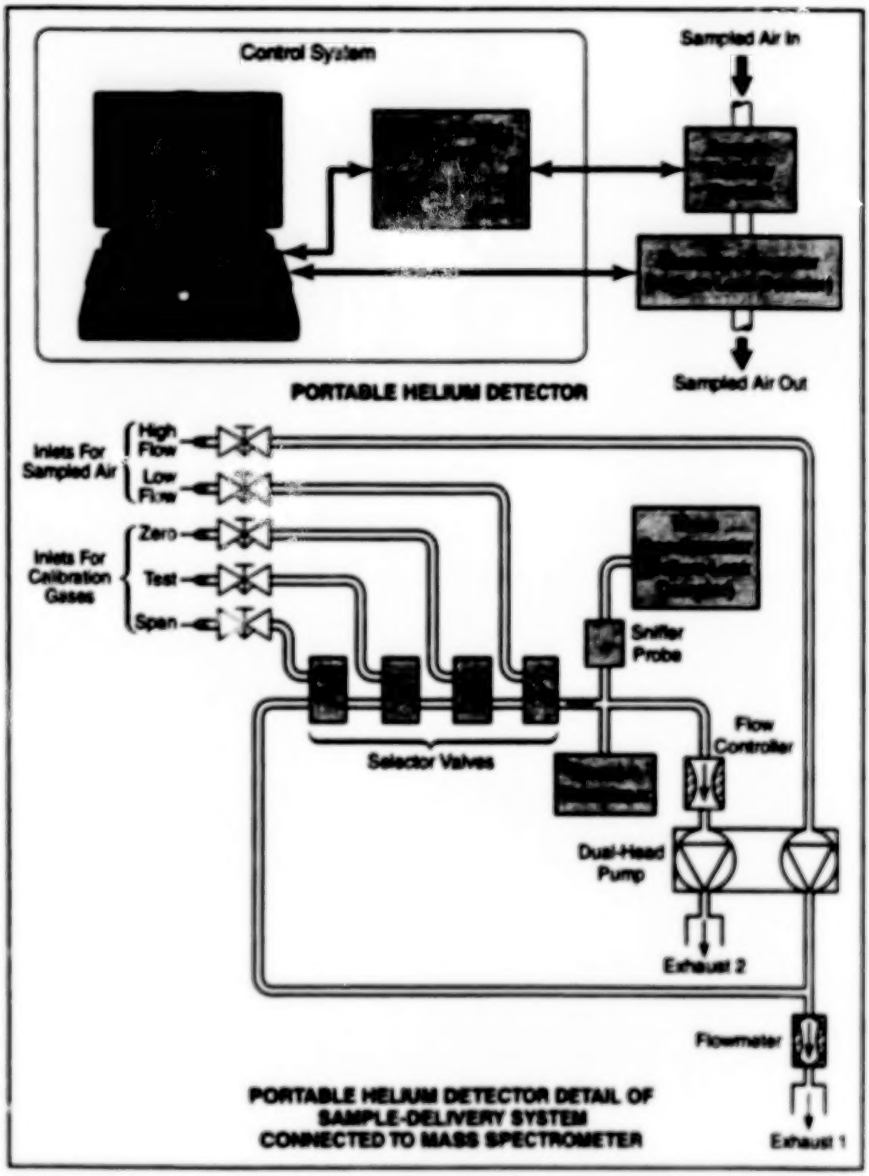

The **Portable Helium Leak Detector** is a cart-mounted system of three modules. One of the modules is the sample-delivery system, which delivers sampled air to the inlet of the mass spectrometer at regulated pressure.

of valves, and the acquisition of data. The computer sends the valve commands to solid-state relays that turn power on and off, as commanded, to control the valves. The output signals from a temperature sensor and from the mass spectrometer are sent to the computer via the analog-to-digital converters.

The software monitors and displays long-term (a test can take several hours) leak trend data and saves all pertinent information on the hard drive of the computer. The software provides options for performing self-calibration and self-leak tests. Control menus on the computer display are grouped as pages or screens that include a setup page, a self-leak-check page, an autocalibration page, and pages dedicated to specific test setups. New pages can readily be added as needed.

The sample-delivery system includes pumps, valves, pressure transducers, and mass-flow controllers, all working together to bring a sample from the atmosphere of interest to the inlet of the mass spectrometer. The sample-delivery system includes two inlets: one for high flow and one for low flow. The high-flow inlet is for use at high volumetric purge flow rates and enables the rapid detection of leaks. The low-flow inlet is for use in tests that involve little or no purge flow.

The most novel aspect of the design of the sample-delivery system is a provision for regulating the pressure at the inlet of the mass spectrometer. The mass spectrometer effectively measures the partial pressure of helium and therefore it is desirable to regulate the total inlet pressure in order to ensure that the measured partial pressure bears a known proportionality to the concentration of helium in the sampled air. The regulation of the inlet pressure is effected by a feedback loop between a pressure transducer and a flow controller. Another unique aspect of the instrument is its ability to be calibrated and provide data as parts-per-million leakage rates. This is done to match the space-shuttle main-engine permissible leakage-rate criteria.

The entire portable leak detector (including the cart) is 23 in. (58 cm) wide, 45 in. (114 cm) high, and 30 in. (76 cm) deep, and has a weight of 346 lb (mass of 157 kg). The three modules can easily be removed to facilitate transport. All three modules are powered via a single 115 Vac outlet.

This work was done by Fredrick Adams, Carolyn Mizell, David Collins, and Gregg Breznik of **Kennedy Space Center**; *Richard Hintz, Francisco Lorenzo-Luaces, Guy Naylor, Curt Lampkin, Timothy Griffin, and Terry Greenfield of Dynacs Engineering Co., Inc.; and Larry Lingvay formerly of I-NET, Inc. Further information is contained in a TSP [see page 1].*
KSC-12054

Liquid Shell Insulation

At high temperatures and pressures, probes would last just long enough to take readings.

NASA's Jet Propulsion Laboratory, Pasadena, California

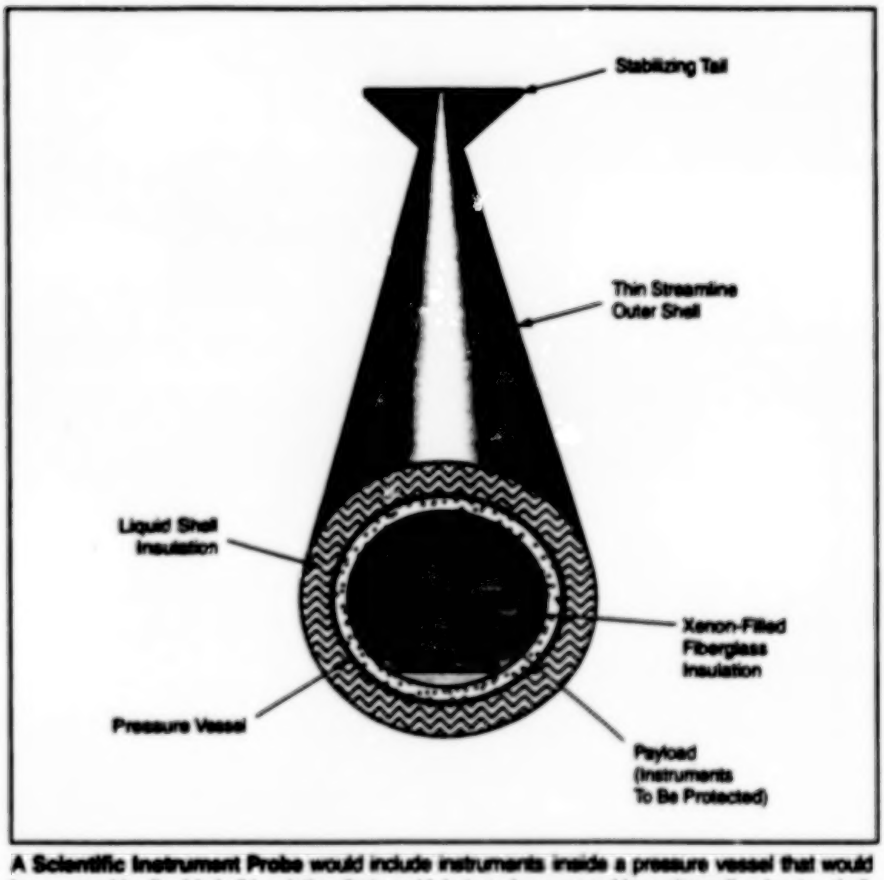

A Scientific Instrument Probe would include instruments inside a pressure vessel that would be covered by liquid shell insulation that would, in turn, be covered by a streamlined outer shell. The liquid shell insulation would provide temporary protection against high ambient temperature.

A new concept called "liquid shell insulation" has been proposed as a means of temporary thermal protection for scientific instrument probes that are required to operate for short times in hot, high-pressure environments. Liquid shell insulation was conceived to protect probes that would be dropped from spacecraft to great depths in the atmospheres of the outer planets. For example, at a depth of 1,000 km on Jupiter, a probe would have to withstand a pressure of about 4,000 Earth atmospheres (≈0.4 GPa) and a temperature of about 1,800 K. On Earth, liquid shell insulation might be useful for protecting probes that would be inserted in undersea volcanic vents or deep oil wells.

The liquid shell insulation would be placed outside the pressure-bearing outer wall of a instrument probe; this would be done so that, in addition to the delicate instrumentation within, the outer wall would also be thermally protected. Thermal protection of the outer wall would be necessary to prevent the crippling loss of mechanical strength that would occur if the wall were allowed to be heated to 1,000 K or more.

As its name suggests, liquid shell insulation would be a shell-like structure, with a liquid-filled porous insulation material surrounding the pressure-bearing outer wall (see figure). The basic function of the liquid shell insulation would be to provide a sufficiently long characteristic thermal time so that the protected instruments would not exceed the maximum allowable temperature after the required collection and transmission of data has occurred. In addition to the liquid shell, the probe would be equipped with a streamlined external shell

for low drag, so that it could descend to the required depth in a minimum time. The inner surface of the pressure vessel would be lined with a secondary insulating layer consisting of fiberglass with xenon gas filling the interstices; this layer would keep the instruments much cooler than the pressure vessel, which, in turn, would be much cooler than the environment.

The design of the liquid shell must combine the following features in order to function properly in a high-pressure, high-temperature environment:

- Low thermal conductivity to limit heating of the pressure vessel,
- High heat capacity to absorb most of the heat conducted in from the environment,
- Equalization of the pressure in the liquid with the ambient pressure to prevent loading of the thin streamlined outer shell,
- Means to prevent hot ambient gases from entering into the shell and compromising its insulating ability.

According to the current design concept, the liquid shell would be made of a porous solid filled with a liquid. To minimize the transfer of heat through the shell, the design and construction of the porous solid component must minimize spurious convective motion of the fluid and attenuate the radiative transfer of heat energy, while allowing some convective motion because of expansion and venting of the liquid as described below.

Both ammonia and water have been considered for use as the liquid. Both of these fluids have very high specific heat capacities and moderate thermal conductivities. Equally important, in the original planetary-exploration scenario, either of these fluids would slowly expand during atmospheric descent because the expansion due to heating would more than offset the shrinkage due to pressurization. Therefore, the shell would have to be open to the atmosphere through a check valve in order to equalize the pressure across the thin streamlined outer shell. The check valve would not only prevent ambient gas from entering the shell, but would also allow the expanding heated liquid to leave the shell, carrying heat with it. Although the liquid ammonia or water would expand during the atmospheric descent, it would not undergo phase change because the ambient pressure would greatly exceed the critical pressure of either fluid [113 atm (11.4 MPa) for ammonia, 220 atm (22.3 MPa) for water].

If ammonia were used, some of it would dissociate into nitrogen and hydrogen at high temperature. The endothermic dissociation reaction would absorb heat, thereby improving the overall insulating performance of the liquid shell.

This work was done by Jeffery L. Hall of Caltech for **NASA's Jet Propulsion Laboratory**. *Further information is contained in a TSP [see page 1].*
NPO-20648

Fluorometer for Analysis of Photosynthesis in Phytoplankton

Measurements could be made *in situ* and *in vivo*.

Stennis Space Center, Mississippi

An instrument that measures the characteristic lifetime of fluorescence of chlorophyll has been invented for *in situ*, real-time oceanographic studies of photosynthesis in phytoplankton. The basic design and principle of operation lend themselves to development of the instrument as a relatively inexpensive, sensitive, compact, rugged, portable, low-power-consumption, hand-held, shipboard unit. Similar units with designs adapted to agricultural applications (e.g., assessment of physiological statuses of crops) are also envisioned.

The need for this or a similar instrument arises because fluorescence lifetimes are robust measures of physical and chemical mechanisms that affect photosynthesis and of the photosynthetic productivity of phytoplankton. The fluorescence lifetimes of particular interest are those associated with fluorescent de-excitation in photosystem II. ("Photosystem II" denotes a series of photosynthetic reactions in which a pigment absorbs light at wavelengths up to 680 nm and absorbed light energy causes the splitting of water molecules, giving rise to oxygen and to a high-energy reductant.) These lifetimes range from about 2 ns down to as little as hundreds of picoseconds. Therefore, in order to exploit the full potential of fluorescence-lifetime measurements for detecting small changes in photosystem-II physiological status, this or any similar instrument would have to exhibit an error <50 ps and a resolution ≈10 ps.

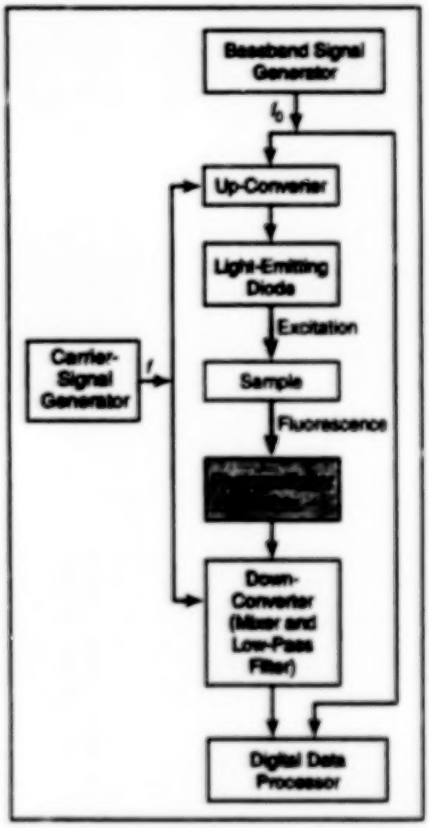

This **Instrument Measures the Phase Difference** between sinusoidally modulated optical excitation and the resulting fluorescence. The fluorescence lifetime is then calculated from the phase difference and the modulation frequency.

The present instrument does not measure fluorescence lifetimes directly; instead, it is based on a principle of phase fluorometry, which can be implemented more easily. In phase fluorometry, a sample is excited with light modulated sinusoidally at an angular frequency ω. The resulting fluorescence emitted by the sample is modulated at the same frequency but, because of the finite lifetime of the excited state, is delayed in phase by an angle ϕ relative to the excitation. The phase angle ϕ is measured and used to calculate a phase lifetime (τ_p) according to $\tau_p = \tan \phi/\omega$. In order to be able to determine τ_p accurately by this method, one must choose a modulation frequency comparable to the rate of decay of the fluorescence.

In the instrument (see figure), a baseband signal of frequency f_0 (typically 600 Hz) is generated for use both as a sample signal and as a reference signal for the phase measurement. Using a single-sideband technique, the sample signal is up-converted by combining it with a carrier signal of frequency f (typically 70 MHz). The up-converted signal (at frequency $f_0 + f$) is used to modulate a light-emitting diode (LED) at wavelength 670 nm), the output of which is used to excite the sample.

The fluorescence emitted by the sample acquires a phase delay that corresponds to a frequency-dependent weighted average

of the lifetimes of the fluorophores present in the sample. The fluorescence, which is modulated at frequency $f_0 + f$, is detected by a photomultiplier tube. The electrical output of the photomultiplier is down-converted to f_0 by mixing it with the carrier signal and low-pass filtering the product signal. The phase information acquired by the up-converted signal through interaction with the sample is preserved in the down-converted signal. The phase-shifted down-converted f_0 sample signal and the reference f_0 signal are captured by an analog-to-digital converter, and the output of the analog-to-digital converter is stored and processed to determine ϕ and τ_p.

This work was done by Salvador M. Fernandez, Ernest F. Guignon, Robert Kersten, and Ernest St. Louis of Ciencia, Inc., for **Stennis Space Center**. *Further information is contained in a TSP [see page 1].*

In accordance with Public Law 96-517, the contractor has elected to retain title to this invention. Inquiries concerning rights for its commercial use should be addressed to

Ciencia, Inc.
111 Roberts Street
Suite K
East Hartford, CT 06108

Refer to SSC-00110, volume and number of this NASA Tech Briefs issue, and the page number.

Improved Illumination Device for Inspecting Window Surfaces

Efficiency of coupling is increased and stray light is reduced.

John F. Kennedy Space Center, Florida

A fiber-optic illumination device that aids the inspection of window surfaces has been improved to make it suitable for automated detection of pits, scratches, and subsurface damage by use of a machine-vision and image-analysis system. The improvements, which include modifications in both the optical and mechanical aspects of its design, significantly reduce the brightness of stray light that, previously, was bright enough to interfere with automated detection of defects.

The previous version of the device (see Figure 1) was described in "Illumination Device for Inspecting Window Surfaces," *NASA Tech Briefs*, Vol. 22, No. 11 (November 1998), page 68. The device could be temporarily attached to a window by use of suction cups. The device coupled light from a fiber-optic cable, through a block of clear material, into the window pane to create a side-lighting effect. One advantage of this or a similar lighting scheme is that light remains within the window because of total internal reflection, except at sites of surface or subsurface defects. Hence, the defects appear bright on an otherwise dark window surface and could be readily observed. Another advantage of this lighting scheme is its selectivity: The more important deep defects present larger cross sections to side illumination than do shallow defects of the same lateral dimensions and therefore tend to appear brighter. Furthermore, dirt particles on the surface, which do not constitute defects in the window and are thus unimportant for purposes of this type of inspection, may couple some light out of the window but they also shield the observer from this light. Hence dirt tends to appear dim, and the incidence of false detections of defects is lower than it would be if a different lighting scheme were used.

A human inspector can distinguish between foreground and background light

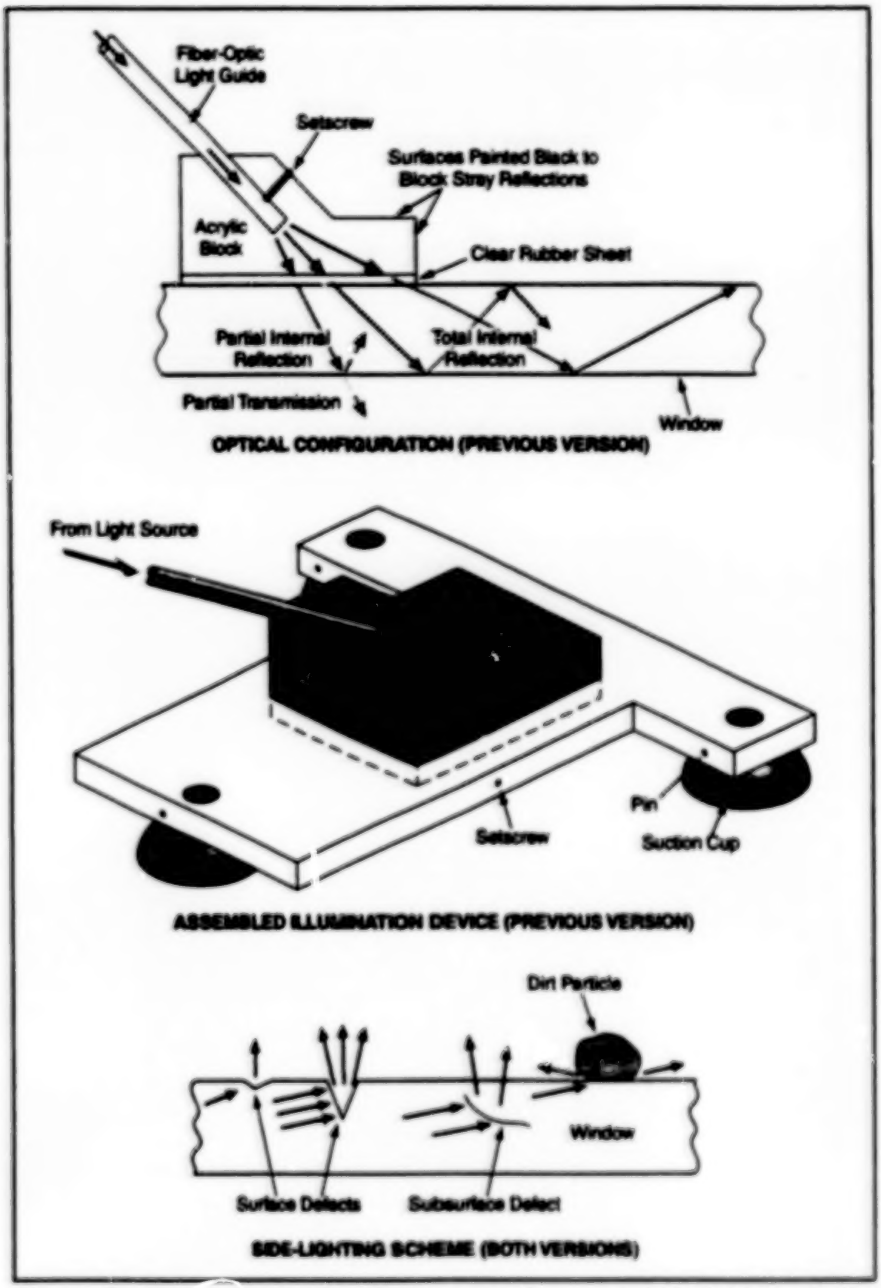

Figure 1. The Previous Version of the Device created the same desired side-lighting effect as does the present version. However, the previous version generated too much stray light to be useful for automated detection of defects.

by, among other actions, refocusing at different depths and changing the angle of observation; however, an automated defect-detection system cannot do this. Therefore, to ensure high sensitivity and consistent performance in an automated defect-detection system, it is necessary to minimize background light, including stray light generated by the illumination device.

The previous version of the illumination device generated appreciable stray light because of two weaknesses in its design. The first weakness was that a significant fraction of light was not subject to total internal reflection in the window. The second weakness was that a significant amount of light was scattered by partial reflection at (1) the interface between the acrylic block and the window and (2) the end of the fiber-optic light guide and the adjacent poor-optical-quality surface at the bottom of the light-guide hole in the acrylic block.

The improved design overcomes these weaknesses. The acrylic block of the previous design is replaced with a triangular prism (see Figure 2) that is shaped and dimensioned to minimize undesired scattering and maximize the amount of light subject to total internal reflection. Light from the fiber-optic light guide enters the prism through the smallest prism face, which is nearly perpendicular to the window surface. Unlike the bottom of the hole in the acrylic block of the previous version, this prism face is accessible prior to assembly, and can therefore be polished to minimize scattering.

The angle of the fiber-optic light guide is adjusted so that even the light rays that enter the window pane most steeply (e.g., ray A in Figure 2) are subject to total internal reflection. Because of the large angular spread of light leaving the fiber-optic light guide, some rays (e.g., ray C in Figure 2) go toward surface c' the prism, where they are

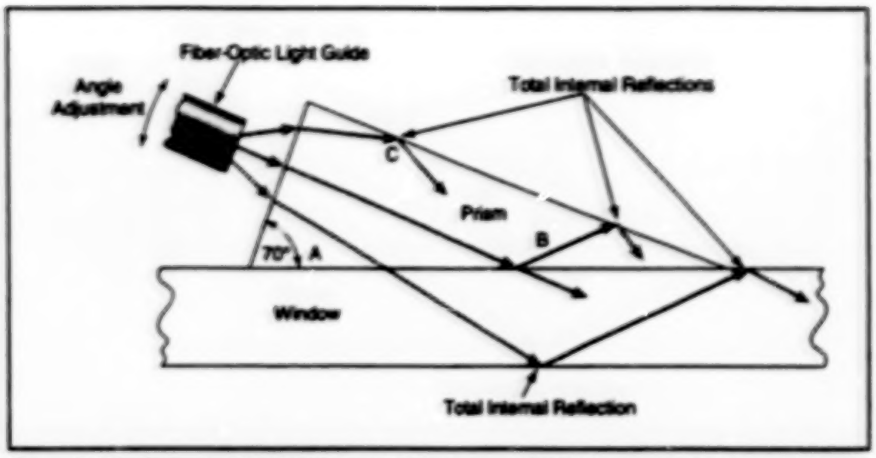

Figure 2. The Improved Optical Layout of the present design increases the amount of light coupled into the window and reduces the amount of stray light.

reflected downward toward the window pane. Proper choice of the prism angles ensures total internal reflection both at the top surface of the prism and the bottom surface of the window pane.

Because of a small mismatch of the indices of refraction of the prism and window, a small fraction of rays is reflected at the prism/window interface (e.g., ray B in Figure 2). In the previous version, these rays contributed to stray light. In the present version, these rays are reflected from the top surface of the prism back toward the window.

The prism must be made short enough to prevent coupling out of rays that have been reflected once from the bottom surface of the window. The maximum length permitted by this criterion depends on the thickness and the index of refraction of the window.

Going beyond purely optical considerations, another disadvantage of the previous version of the device was that as the suction cups gradually relaxed, a gap of approximately 1 mm developed between the window surface and either the acrylic block or (if used) the clear rubber sheet attached to the acrylic block. It was necessary to fill the gap with an index-of-refraction-matching liquid, which could easily run out or evaporate under the heat of the illumination, making the device unreliable after a short time.

In the improved version, the prism is mounted in a frame with a free range of motion, >1 mm, that makes it possible for the prism to remain in contact with the window. After attaching the device to the window by use of the suction cups, one pushes specially shaped wedge slides between parts of the prism and the frame. This action stretches the suction cups, providing sufficient force to ensure steady contact, thereby retarding the loss of coupling fluid. The net result is that the device provides reliable and constant lighting with minimum background illumination suitable for automated inspection of windows.

This work was done by Henry Weidner, Terry Greenfield, and Carl Hallberg of Dynacs Engineering Co. and Anthony Krsljic of United Space Alliance for **Kennedy Space Center**. *Further information is contained in a TSP [see page 1].*
KSC-12127

Gas Analyzer Measures Concentrations of H_2, O_2, and H_2O

This apparatus can help ensure safety in a system that handles liquid hydrogen.

John F. Kennedy Space Center, Florida

An apparatus measures small concentrations of H_2, O_2, and H_2O in flowing He gas. In the original application for which the apparatus was developed, the flow of He gas is used to purge a tube through which liquid hydrogen is transferred:

- The tube must be purged to remove water vapor and oxygen prior to the introduction of liquid hydrogen into the tube; hence, it is necessary to verify that O_2 and H_2O are no longer present in the purge gas before stopping this purge.
- Once the transfer of hydrogen through the tube is complete, the tube must be purged to remove hydrogen; hence, it is necessary to verify that H_2 is no longer present in the purge gas before stopping this purge.

The apparatus could also be used to measure concentrations of H_2, O_2, and/or H_2O in other cryogenic-liquid or gas systems.

The apparatus (see figure) includes H_2, O_2, and H_2O sensors; a sampling pump; flow controllers; a pressure transducer; a thermocouple; a computer; a display panel; and a modem. The H_2 and O_2 sensors can measure concentrations from 0 to 10 percent with accuracies of ±1 percent of their full-scale readings and can withstand sound and vibration conditions of a space shuttle launch. The H_2 sensor can operate at temperatures from −10 to +60 °C; the O_2 sensor can operate at tem-

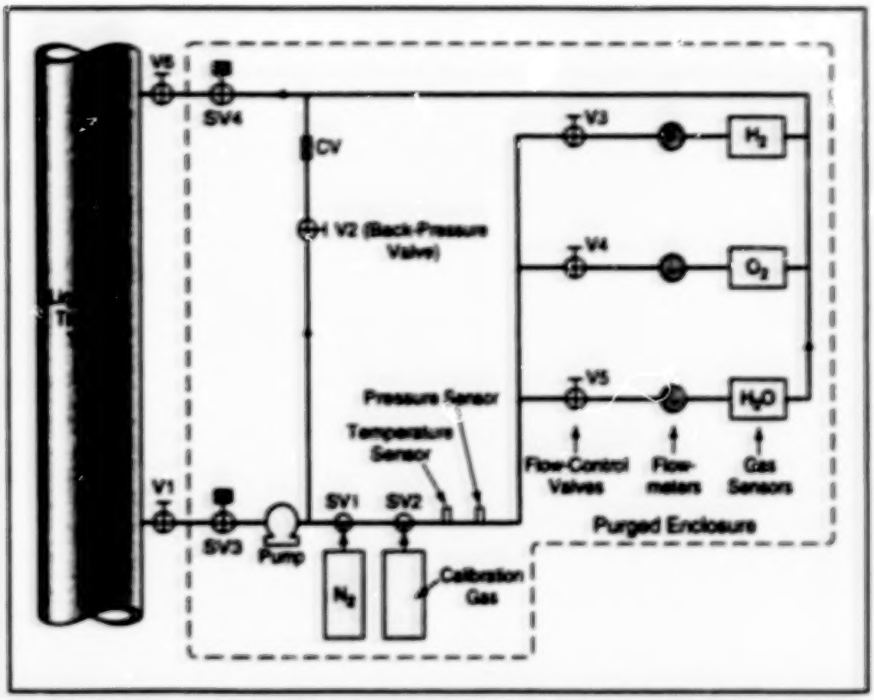

The Gas Analyzer measures the concentrations of H_2, O_2, and H_2O in the liquid-H_2-transfer tube while the tube is undergoing a purge with He.

peratures from −10 to +40 °C. The H_2O sensor can measure concentrations from 125 parts per million (ppm) to 4 percent, with an accuracy of ±10 ppm at 125 ppm. The H_2O sensor can operate at temperatures from −10 to +40 °C.

The computer, modem, and display panel are used to control the operation of the rest of the apparatus and to interpret the sensor readings. Control and monitoring tasks can be performed at a safe location, remote from the sensors and the gas system during hazardous operations (e.g., operations in which significant quantities of both hydrogen and oxygen could be present).

The apparatus can be isolated from, or connected to, the purged liquid-hydrogen-transfer tube by use of manual valves V1 and V6. Once these valves have been opened, the apparatus operates in the following sequence:

1. Solenoid valves SV3 and SV4 are opened.
2. The plumbing of the apparatus is purged with N_2 to remove traces of H_2O water vapor that may have leaked in.
3. After the N_2 purge, the sampling pump is started. The pump pulls a sample of gas from the liquid-hydrogen-transfer tube through SV3, then pushes through the flow-control valves, flowmeters, and gas sensors. After passing through the gas sensors, the sampled gas is returned through SV4 back into the liquid-hydrogen-transfer tube.

The apparatus continuously measures the concentrations of H_2, O_2, and H_2O; the rates of flow in the three sensor lines; and the pressure and temperature of the sample gas. All data are logged on a host computer and displayed at a control station. The apparatus can be calibrated from either a remote control station or from a control panel on the apparatus.

This work was done by Clyde F. Parrish, Christian J. Schwindt, Steven J. Klinko, and Timothy R. Hodge of Dynacs Engineering Co., Inc., for **Kennedy Space Center**. *Further information is contained in a TSP [see page 1].*
KSC-12136

Phonon-Assisted Quantum-Well Infrared Photodetector

Dark current would be reduced by a unique dual-quantum-well structure.

NASA's Jet Propulsion Laboratory, Pasadena, California

A proposed quantum-well infrared photodetector (QWIP) would exploit resonant-phonon-assisted transitions to reduce dark current significantly below that of a typical previously developed QWIP operating at the same wavelength and temperature. The reduction in dark current would translate to greater sensitivity, a capability to measure the diminished infrared radiation from cooler objects, and/or a less severe requirement for cooling an infrared sensor to obtain a desired signal-to-noise ratio.

The proposed QWIP would likely be fabricated by molecular-beam epitaxy of alternating layers of doped GaAs and $Al_xGa_{1-x}As$ on a semi-insulating GaAs substrate. The thicknesses and compositions of the GaAs and $Al_xGa_{1-x}As$ layers would be chosen to form a stack of 25 pairs of coupled quantum wells. The depths and thicknesses of the wells, the thickness of the barrier between the wells in each pair, and the bias electric field to be applied during operation would be chosen to (1) promote excitation of electrons through absorption of photons in the infrared wavelength range of interest and (2) increase (relative to previously developed QWIPs) the heights of the energy barriers to thermionic emission, which is the dominant source of dark current in the temperature range of interest (≤55 K).

The figure is a conduction-band energy diagram of one pair of quantum wells. The wells would be engineered so that at the threshold applied electric field, $E_2-E_1 = \Delta E_{ph}$, where ΔE_{ph} is an optical-phonon energy. Barrier heights and well thicknesses would be chosen such that the photoexcitation energy between ground and first excited states in both wells would the same; that is, $E_3-E_1 = E_4-E_2 = \Delta E_{ex}$, where ΔE_{ex} is the photoexcitation energy (photon energy) at the desired wavelength of peak detector response. In addition, E_4 — the first excited state of the right well — would be placed exactly at the top of the well.

The ground state of the left quantum well would be doped up to Fermi level E_F, which would be below E_2. Electrons in the E_1 level would become excited to the E_3 level by absorbing photons. The stated engineered relationships among the energy levels at the threshold electric field would give rise to resonance between (1) the transition from E_3 to E_2 and (2) the optical phonon without (3) transfer of momentum. Consequently, an electron that had been photoexcited from E_1 to E_3 would make a rapid transition (within a typical quantum-state lifetime of the order of a picosecond) from E_3 to E_2. Repeated such excitations and transitions would cause the ground (E_2) state of the

right potential well to become populated.

The lifetime of the E_2 level would exceed that of the E_3 level because decay back to E_1 would involve emission of an optical phonon with a large transfer of momentum. The lifetime of the E_2 level would be long enough that an electron in that level would have a high probability of absorbing a second photon, thereby gaining enough energy to escape from the right well to be collected as photocharge. Optimization of design would involve balancing of these various quantum transition processes while providing for coupling of radiation of the wavelength of interest to electrons in the quantum wells.

The quantum efficiency of the proposed QWIP would be about half or even less than half of that of a typical previously developed QWIP, because now two photons would have to be absorbed to get one electron out. However, there would still be a net increase in signal-to-noise ratio because effective height of the barrier against thermionic emission would be increased sufficiently that the dark current would be reduced to much less than half of the previous value. For example, it has been estimated that for a wavelength of 15 μm (equivalent to a photon energy of about 82 meV), an optical-phonon energy of about 36 meV, and a temperature of 55 K, the dark current of the proposed QWIP would be about a thousandth of that a typical previously developed QWIP.

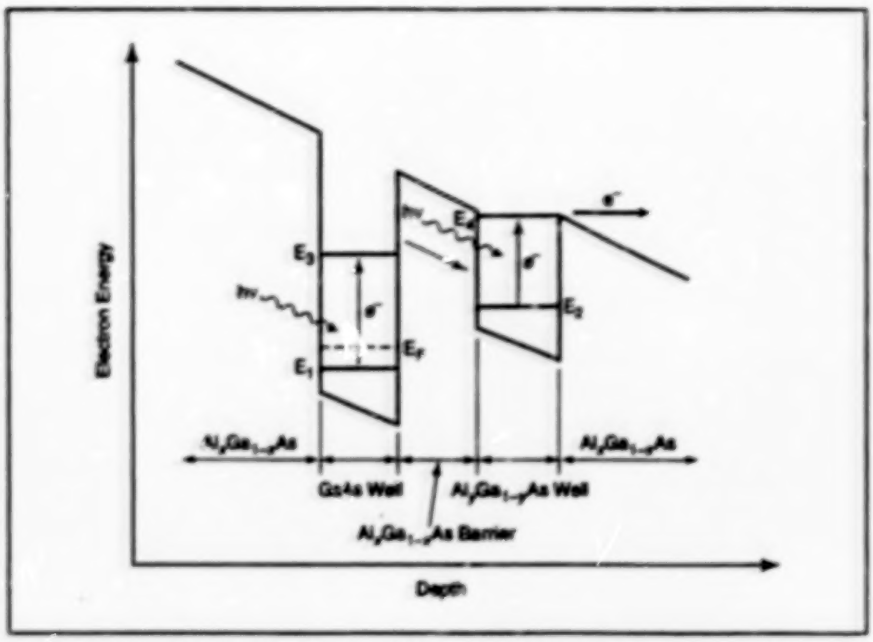

The Energy Levels in the Two Quantum Wells and the barrier between them would be chosen to impose high barriers against thermionic emission and thermionic tunneling, without hindering the escape of photoexcited electrons from the right well to the continuum. The wavy lines represent the absorption of photons.

This work was done by Sumith Bandara, Sarath Gunapala, and John K. Liu of Caltech for **NASA's Jet Propulsion Laboratory**. *Further information is contained in a TSP [see page 1].*

In accordance with Public Law 96-517, the contractor has elected to retain title to this invention. Inquiries concerning rights for its commercial use should be addressed to

Technology Reporting Office
JPL
Mail Stop 122-116
4800 Oak Grove Drive
Pasadena, CA 91109
(818) 354-2240

Refer to NPO-20568, volume and number of this NASA Tech Briefs issue, and the page number.

Coupling Light Between Optical Fibers and Noncircular Beams

Cylindrical lenses are used to change aspect ratios.

NASA's Jet Propulsion Laboratory, Pasadena, California

Cylindrical lenses can be used to increase the efficiency of coupling of light between (1) beams with circular or nearly circular cross sections propagating in single-mode optical fibers and (2) free-space beams with noncircular cross sections and with different radii of curvature of wavefronts on mutually perpendicular meridional planes. Beams of the second type are generated by semiconductor optoelectronic devices (e.g., diode lasers and amplifiers) that contain stripe waveguides; the waist-cross-section aspect ratios of such beams can be as large as 3:1.

Heretofore, it has been common practice to use anamorphic prism pairs to change aspect ratios of light beams entering and leaving single-mode optical fibers. It is also possible, in principle, to change beam aspect ratios by use of cylindrical lenses mounted within diode laser packages. Both of these approaches entail disadvantages: Anamorphic prism pairs are bulky and introduce insertion losses of about 10 percent, and it is often not practical to modify diode laser packages to incorporate cylindrical lenses. However, it

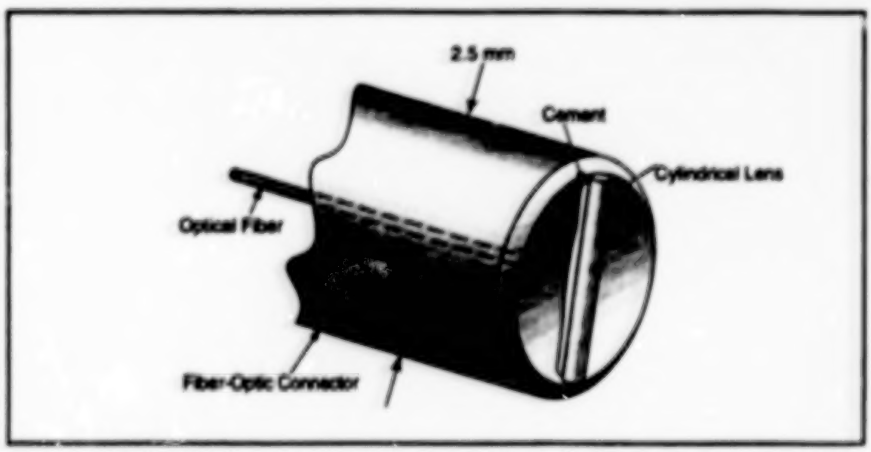

Figure 1. A Cylindrical Lens is cemented to the end faces of a fiber-optic connector and the fiber held by the connector.

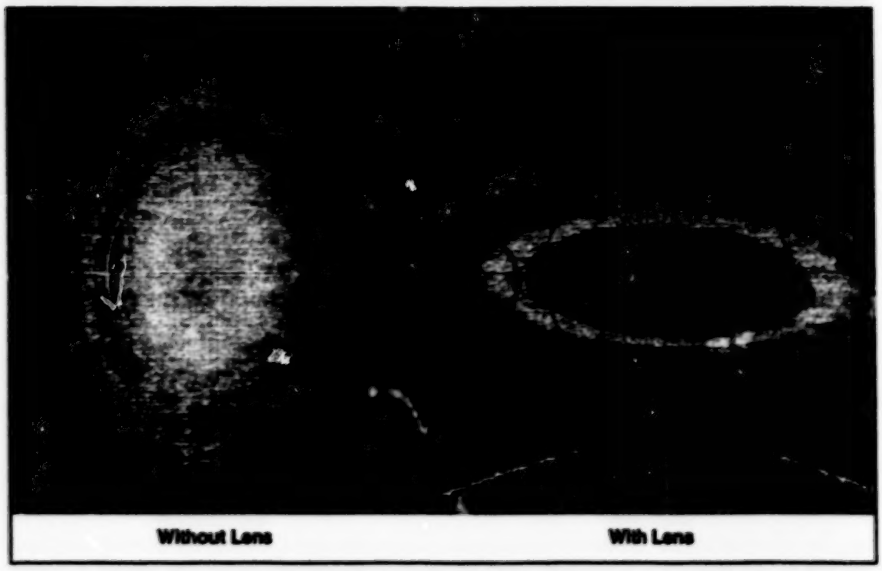

Figure 2. These Are Cross-Sectional Images of Light Beams at a wavelength of 852 nm emerging from the end of a polarization-maintaining optical fiber of aspect ratio 0.8, without and with a cylindrical lens. The lens converted the aspect ratio to 2.9. The insertion loss in the presence of the lens was only 3 percent.

is practical to mount cylindrical lenses on the ends of optical fibers.

The cylindrical lens for a typical application is made of a suitable glass and is designed to be glued to the end face of a connector that holds the optical fiber (see Figure 1) by use of an ultraviolet-curable cement that matches the index of refraction of the fiber, the lens, or both. In conjunction with the indices of refraction of the fiber and lens glasses, the diameter of the lens and its nominal small distance from the end face of the fiber are chosen to obtain the required conversion of wavefront curvature in the affected plane. The design provides that any gap between the lens and the end face of the fiber be filled with the cement.

In preparation for mounting the cylindrical lens on the end of the fiber, light of the wavelength of interest is coupled into the fiber at one end and a video camera sensitive to light at that wavelength is positioned to obtain a cross-sectional image of the beam of light emerging from the end of the fiber. The cylindrical lens is placed on a three-dimensional translation stage and moved to approximately the desired position near the end of the fiber. The gap between the cylindrical lens and the end face of the fiber is filled with cement, but not with so much that the cement could overflow and cover the free-space side of the lens. Then by use of the translation stage, the lens is maneuvered precisely into position on or near the end face of the optical fiber. The maneuvers are continued until the image exhibits the required aspect ratio and is centered on the optical axis of the fiber (see Figure 2). Then ultraviolet light is applied to cure the adhesive in place.

This work was done by Herbert Pickett and Christopher Mackay of Caltech for **NASA's Jet Propulsion Laboratory**. *Further information is contained in a TSP [see page 1].*

In accordance with Public Law 96-517, the contractor has elected to retain title to this invention. Inquiries concerning rights for its commercial use should be addressed to

Technology Reporting Office
JPL
Mail Stop 122-116
4800 Oak Grove Drive
Pasadena, CA 91109
(818) 354-2240

Refer to NPO-20637, volume and number of this NASA Tech Briefs *issue, and the page number.*

Fast Infrared Spectrometer

This instrument could be useful in research on flames.

John H. Glenn Research Center, Cleveland, Ohio

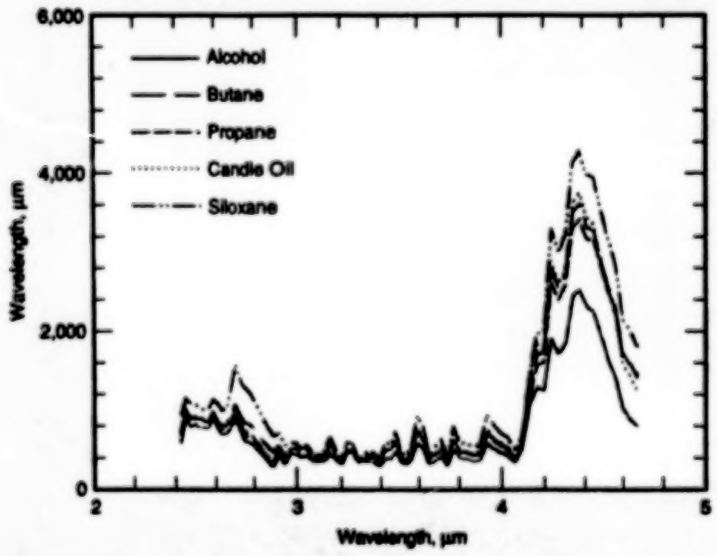

Spectra From Five Flames were measured by the fast infrared spectrometer.

A spectrometer has been developed for acquiring transient emission and absorption spectra in the wavelength range from 1.2 to 5.0 µm. It could be used to characterize flames, turbulence, and other transient phenomena that interact with infrared radiation. Heretofore, success in the study of such phenomena has been limited by the inability of infrared spectrometers to acquire data at sufficiently high speeds. In contrast, the present infrared spectrometer measures the spectrum at a repetition frequency of 390 Hz. The high speed of this instrument could also make it attractive for such commercial applications as monitoring food, pharmaceutical, and petroleum products in process streams and on production lines.

The spectrometer optics include a chopper, two prisms that serve as dispersers, and parabolic optical-path-fold-

ing mirrors. The spectrally dispersed light is projected onto a 160-pixel linear array of lead selenide photodetectors. The spectrometer also includes electronic circuitry for controlling the chopper, synchronizing readout from the pixels with the chopping cycle, and sending data to an external computer or data logger, all at the repetition frequency of 390 Hz.

The spectrometer is housed in an assembly with overall dimensions of 222 by 165 by 89 mm. A data logger for use with the spectrometer in a special application (a drop-tower rig) is mounted in a separate housing with overall dimensions of 432 by 140 by 190 mm. Because of requirements specific to that application, the data logger stores the data on an easily removable Personal Computer Memory Card International Association (PCMCIA) card. The spectrometer with the data logger is the fastest and smallest instrument of its kind.

The spectrometer was calibrated by use of a black-body radiation source at a temperature of 980 K along with narrow-passband filters at wavelengths of 2.56, 2.71, 4.26, and 4.33 μm. In a further calibration experiment, flames fed by alcohol, butane, propane, candle oil, and siloxane were used as radiation sources (see figure). The temperatures of the flames were calculated on the basis of the flame spectra and found to range from 2,175 K for the candle-oil flame to 2,475 K for the alcohol flame. These values are close to the expected adiabatic flame temperatures, and the fact that the lowest temperature was that of the candle flame is consistent with the expectation that the radiative loss from that flame would be greater than from the other flames. Therefore, the calculated temperatures seem reasonable.

This work was done by Yudaya Sivathanu and Rony Joseph of En'Urga Inc. for **Glenn Research Center**.

Inquiries concerning rights for the commercial use of this invention should be addressed to NASA Glenn Research Center, Commercial Technology Office, Attn: Steve Fedor, Mail Stop 4–8, 21000 Brookpark Road, Cleveland, Ohio 44135. Refer to LEW-16784.

Whispering-Gallery-Mode Microspheres as Light Modulators

Ultrahigh modulation efficiency could be achieved.

NASA's Jet Propulsion Laboratory, Pasadena, California

Light modulators of a proposed type would exploit the propagation of light in "whispering-gallery" electromagnetic modes in microspheres made of electro-optical materials. These modulators would offer advantages of ultrahigh modulation efficiency and increased bandwidth, relative to their nearest competitors, which are traveling-wave electro-optical modulators. The introduction of the proposed modulators could increase the bandwidths and reduce the power demands of a variety of both free-space and guided-wave communication, sensing, and signal-processing systems that utilize radio-frequency (typically, microwave) modulation of optical carrier signals.

The whispering-gallery modes of a dielectric microsphere are resonance modes in which electromagnetic fields are confined, by internal reflection, to an interior region within about 10 μm of the surface of the sphere. For a microsphere with a diameter ≥ 10 μm, the dimension of the resonator is much larger than the wavelength of light. Thus, the loss due to the finite curvature of the resonator is negligible, resulting in a resonance quality factor (Q) that is high and is limited mainly by the attenuation of the light in the dielectric material.

An important example is that of a microsphere with a diameter of about 3 mm, made of the electro-optical material lithium niobate. Such a microsphere can support optical whispering-gallery modes at $Q \approx 10^7$. Because its relative permittivity at radio frequencies is about 50, it can also support microwave and millimeter-wave whispering-gallery modes at $Q \approx 10^4$. These characteristics are favorable for use of the microsphere as a radio-frequency light modulator.

In the proposed modulation scheme, one would apply a radio-frequency (microwave or millimeter-wave) field to a microsphere in which an optical signal propagates in a whispering-gallery mode. Acting via the electro-optical effect, the electric component of the radio-frequency field would alter the speed of propagation of, and thereby modulate, the optical signal. With a proper choice of design parameters, the radio-frequency field could be concentrated in a whispering-gallery mode in the same near-surface interior region as that of the optical whispering-gallery mode. Because of the high Q values, the circumferential path along which the radio-frequency and optical fields would propagate and interact via the electro-optical effect would be > 1 km long; in contrast, the interaction lengths in typical traveling-wave electro-optical modulators range from a few millimeters to a centimeter.

The increase in the effective interaction length would reduce the change in index of refraction needed to obtain a given depth of modulation in a microsphere electro-optical modulator to about 10^{-6} that needed to obtain the same depth of modulation in a traveling-wave electro-optical modulator. The net effect is that the order of magnitude of modulation potentials for microsphere electro-optical modulators would be millivolts, as compared with volts for traveling-wave electro-optical modulators. Even after accounting for inefficiencies in the coupling of optical and radio signals between a microsphere and the other optical and electronic components, microsphere electro-optical modulators are expected to be orders of magnitude more efficient than are traveling-wave electro-optical modulators. Moreover, it has been estimated that the maximum useable modulation frequency would be increased from ≈50 GHz in the traveling-wave case to ≈100 GHz in the microsphere case.

This work was done by Lute Maleki, Anthony F. J. Levi, X. Steve Yao, and Vladimir Iltchenko of Caltech for **NASA's Jet Propulsion Laboratory**. *Further information is contained in a TSP* *[see page 1]*.

In accordance with Public Law 96-517, the contractor has elected to retain title to this invention. Inquiries concerning rights for its commercial use should be addressed to

Technology Reporting Office
JPL
Mail Stop 122-116
4800 Oak Grove Drive
Pasadena, CA 91109
(818) 354-2240

Refer to NPO-20664, volume and number of this NASA Tech Briefs *issue, and the page number.*

Magnetostrictive Heat Switches Actuated by Flux Tubes

A switch would remain "open" or "closed" until actuated to change its state.

NASA's Jet Propulsion Laboratory, Pasadena, California

In a proposed improvement on the basic concept of a magnetostrictive heat switch for cryogenic applications, the magnetic field needed for actuation would be generated by a superconducting flux tube (SFT). A closely related concept for a magnetostrictive heat switch was presented in "Magnetostrictive Heat Switch for Cryogenic Use" (NPO-20274), *NASA Tech Briefs*, Vol. 23, No. 8, [August, 1999] p. 48. To recapitulate: The main thermal contact in the heat switch would be made or broken by making or breaking, respectively, the mechanical contact between (1) the moving end of a rod of magnetostrictive material and (2) a fixed contact pad. The magnetic field needed for actuation would be generated by use of a superconducting solenoid.

The use of an SFT instead of a superconducting solenoid would be a significant and advantageous departure from the earlier proposal. In the case of a solenoid, it would be necessary to supply current continuously to the solenoid to maintain the magnetic field needed to keep the switch in either the "open" or "closed" state; turning off the current in the solenoid would cause the switch to revert to the opposite state. In contrast, in the case of an SFT, the magnetic flux would remain constant without power applied (other than the separate power needed in any event to maintain the cryogenic environment). Thus, an SFT-actuated heat switch would be bistable; it would remain in either the "open" or "closed" state until toggled into the opposite state. Toggling would be effected by applying a pulsed current to a coil around the SFT to change the magnetic flux and thereby change the degree of magnetostriction.

In comparison with externally actuated mechanical and gas-gap heat switches, both the superconducting-solenoid SFT-type magnetostrictive heat switches would offer the advantage of less heat leakage. Both magnetostrictive heat switches would function at the temperatures of the devices to be thermally switched, with little or no thermal hysteresis. The switching time of either magnetostrictive heat switch would be only about one thousandth of that of a gas-gap heat switch. The SFT-actuated switch would offer the additional advantage that in the steady state, any thermal disturbance that it would introduce would be almost unmeasurably small and, in most cases, completely negligible.

SFTs made of bismuth strontium calcium copper oxide (BSCCO) are already available. Typical lengths and outer diameters are of the order of centimeters, and bore diameters range upward from 1 cm. Flux densities range from 0 to 10 T in the approximate temperature range from 77 K (liquid nitrogen) to 4 K (liquid helium). These flux densities are more than adequate for a magnetostrictive heat switch; the range of flux densities for magnetostrictive materials that have been investigated for use in heat switches is 0 to 0.2 T in the given temperature range.

This work was done by Robert Chave of Caltech for **NASA's Jet Propulsion Laboratory.** *Further information is contained in a TSP [see page 1].*

NPO-20502

Magnetostrictive Valves Actuated by Flux Tubes

Power would be applied during toggling only.

NASA's Jet Propulsion Laboratory, Pasadena, California

Magnetostrictive valves for cryogenic applications would be actuated by superconducting flux tubes (SFTs), according to a proposal. The reasoning behind this proposal closely tracks that of the proposal to use SFTs in magnetostrictive heat switches, as reported in the preceding article.

Previous versions of magnetostrictive valves for cryogenic applications were described in "Magnetostrictive Valve for Use at Low Temperature" (NPO-19480), *NASA Tech Briefs*, Vol. 21, No. 2 (February 1997), page 14b and "Improved Magnetostrictive Valve for Use at Low Temperature" (NPO-20271), *NASA Tech Briefs*, Vol. 23, No. 8 [August, 1999], page 48. As in magnetostrictive heat switches, the actuators in magnetostrictive valves are magnetostrictive rods, and actuation is effected by turning magnetic fields on or off.

Magnetostrictive valves are useful primarily in cryogenic instrumentation. They are especially useful for controlling flows of liquid helium. Typically, a magnetostrictive valve is required to operate in a normally closed (energize-for-flow) mode. The magnetic fields needed for actuation of magnetostrictive valves like those reported previously can be generated by either normally conductive or superconductive solenoidal coils. It is necessary to supply current continuously to the solenoids to maintain the magnetic fields needed to keep the valves open.

SFTs for magnetostrictive valves could be made of bismuth strontium calcium copper oxide (BSCCO), as described in more detail in the preceding article. As in the case of a magnetostrictive heat switch, the main advantage of using an SFT (instead of a solenoid) to actuate a magnetostrictive valve is that the valve would remain in either the "open" or "closed" state until toggled into the opposite state by applying a pulsed current to a coil around the SFT to change the magnetic flux and thereby change the degree of magnetostriction. It may even be possible to select flux levels corresponding to states intermediate between "open" and "closed" to regulate flow; in that case, the valve would remain in the selected flow state, without power applied, until actuated into the next state.

The advantages of magnetostrictive valves actuated by either superconducting solenoids or SFTs are almost identical to those of similarly actuated magnetostrictive heat switches; low heat leakage, little or no thermal hysteresis, and functionality at the temperatures of the flows to be controlled. Valves actuated hydraulically with helium as the hydraulic fluid offer flow control with minimal thermal perturbation of cryogenic environments, but operate with response times about 100 times those of magnetostrictive valves.

This work was done by Robert Chave of Caltech for **NASA's Jet Propulsion Laboratory.** *Further information is contained in a TSP [see page 1].*

NPO-20503

Fiber-Optic Sensors for Measuring Oxygen Dissolved in Water

Colors of immobilized metal complexes change in the presence of dissolved oxygen.

John F. Kennedy Space Center, Florida

Fiber-optic sensors for measuring concentrations of oxygen dissolved in water are undergoing development. In comparison with electrochemical dissolved-oxygen sensors, the fiber-optic sensors are expected to be easier to use and maintain. Also, unlike electrochemical dissolved-oxygen sensors, the fiber-optic dissolved-oxygen sensors are amendable to connection into networks for taking measurements at multiple sites.

The fiber-optic sensors detect oxygen through changes in color. A sensor of this type includes an optical fiber coated with an oxygen-conducting polymer matrix. Specific metal complexes that exhibit rapid and reversible binding of oxygen with associated changes in optical absorption spectra are immobilized in the polymer matrix. In operation, the coated fiber is immersed in water at a test site, and by use of optoelectronic components coupled with the optical fiber, the absorption spectrum of the metal complexes in the coating is measured. The absorption spectrum is then translated into the concentration of dissolved oxygen.

The absorption-measurement principle of the developmental fiber-optic sensors is compatible with a network of distributed sensors and results in lower costs of instrumentation.

This work was done by Michael Schwartz of Eltron Research, Inc., for **Kennedy Space Center**. *Inquiries should be addressed to Michael T. Carter, Eltron Research, Inc., 4600 Nautilus Ct. South, Boulder, CO 80301; telephone (303) 530-0263.*

In accordance with Public Law 96-517, the contractor has elected to retain title to this invention. Inquiries concerning rights for its commercial use should be addressed to the above. Refer to KSC-11999, volume and number of this NASA Tech Briefs *issue, and the page number.*

Buoy Instrumented for Spectral Measurement of Water Quality

An instrumented buoy measures selected aspects of the spectrum of upwelling light for assessment of "water quality." The buoy carries a previously patented optical-backscatter probe that contains a hyperspectral sensor. The output of the probe is processed by a small onboard computer. Cellular-telephone circuitry on the buoy transmits spectral-signature data to a computer system that, in turn, makes the data available immediately over the World Wide Web. Power is supplied by gel batteries charged by a solar photovoltaic panel on top of the buoy. The scalable optical-backscatter probe is a scalable module fabricated separately from the buoy and the other equipment described above; the buoy and the other equipment are designed to accommodate and mate with the optical probe. Optionally, the instrumentation on the buoy can be augmented by incorporation of additional sensors (e.g., a pH sensor current meter). The current version of the buoy is not intended to function in the presence of high wind and waves; it is designed primarily for operation under relatively calm-sea conditions in shallow, semienclosed natural bodies of water (ponds, lakes, lagoons).

This work was done by Charles Bostater of Florida Institute of Technology for **Kennedy Space Center**. *For further information, please contact http://www.ocn.fit.edu/buoy. KSC-12053*

32

BLANK PAGE

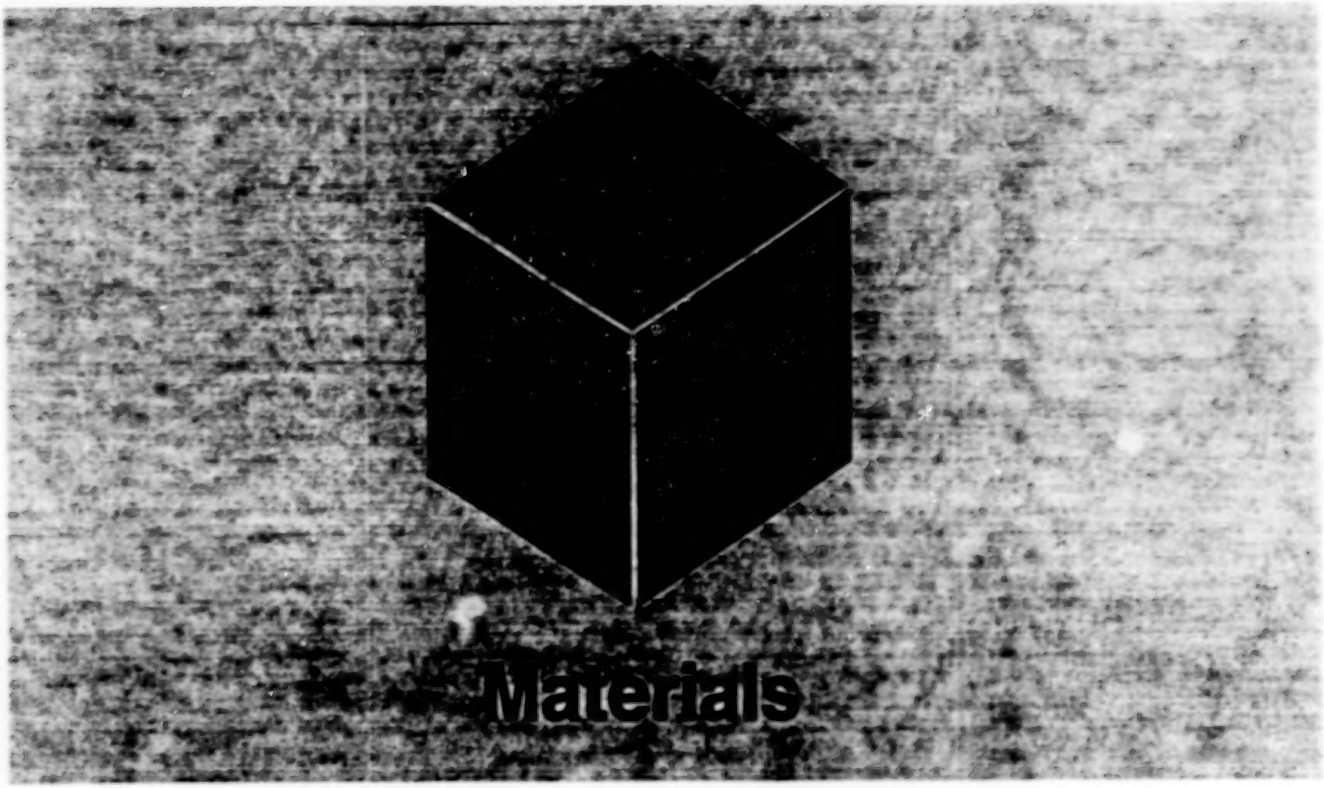

Hardware, Techniques, and Processes

35 Improved Coatings for Flexible Insulating Blankets
35 Polyaniline Compounds for Protection Against Corrosion
36 PBO Fiber Blends: A Promise for the Future
37 Electrodeposition of Strong Glassy Metals

BLANK PAGE

Improved Coatings for Flexible Insulating Blankets

These materials offer increased resistance to erosion.

Lyndon B. Johnson Space Center, Houston, Texas

"ACE" (for "advanced ceramic engineered") denotes a type of coating material that increases the ability of flexible thermal-insulation blankets to resist erosion. Developed for use on the insulating blankets on the space shuttle orbiters, these coating materials could also be used on similar terrestrial insulating blankets on aircraft, engine, and furnace components.

ACE coatings are available in two varieties; a white reflectance coating or a gray emittance coating. The white variety is formulated with (1) a binder of tetraethylorthosilicate (TEOS), which is a polymeric precursor to silica and (2) a filler of high-purity silica powder. The gray variety is formulated with the same binder and filler, but also contains silicon carbide as an emittance agent.

The ACE coatings are similar to a coating material called "C-9" that has been used on the space shuttle insulating blankets. (The binder in C-9 is a colloidal silica.) In preliminary rain erosion tests and in consecutive radiant-heat and air-jet erosion tests, ACE coatings resisted erosion better than C-9 coatings did.

This work was done by Mary M. Fleming and Gordon R. Toombs of Rockwell International Corp. for **Johnson Space Center.**

Title to this invention has been waived under the provisions of the National Aeronautics and Space Act (42 U.S.C. 2457(f)), to Rockwell International Corp. Inquiries concerning licenses for its commercial development should be addressed to

Rockwell World Headquarters
777 East Wisconsin Avenue,
Suite 1400
Milwaukee, WI 53202

Refer to MSC-22495, volume and number of this NASA Tech Briefs issue, and the page number.

Polyaniline Compounds for Protection Against Corrosion

Protective surface layers can be formulated and applied in various ways.

Lyndon B. Johnson Space Center, Houston, Texas

Corrosion of iron and steel substrates can be inhibited by coating them with any of the wide variety of compounds denoted generally as polyanilines. A polyaniline suitable for this type of application can be in either an electrically conductive salt (doped) form or an electrically nonconductive base form. Typically, polyaniline is dissolved in an organic solvent and the resulting solution is applied to a substrate by spraying, dipping, or brushing. The solvent is then allowed to evaporate leaving the substrate coated with a solid film of polyaniline, typically 1 to 200 μm thick.

The figure illustrates the general molecular structures of aniline monomers and polymers. In general, the synthesis of a polyaniline involves mixing an aniline monomer with a protonic acid (e.g., hydrochloric acid), and a polymerization agent in an aqueous medium. The mixture is stirred and maintained at a temperature that depends upon the specific formulation and is typically a few degrees above or below 0 °C. The polymer forms as a blue-green precipitate, which is collected.

The polyaniline precipitate is washed with a protonic acid and/or organic solvent to obtain a polyaniline salt with a molecular structure like that shown in the second part of the figure. If desired, the polyaniline salt can be treated with an aqueous base (e.g., ammonium hydroxide) to convert the salt to a base with a molecular structure like that shown in the third part of the figure. The resulting polyaniline base is preferably in an oxidation state associated with a form of polyaniline called "emeraldine." The polyaniline base can then be recovered by such established techniques as washing with an aqueous base and organic solvents, followed by vacuum drying.

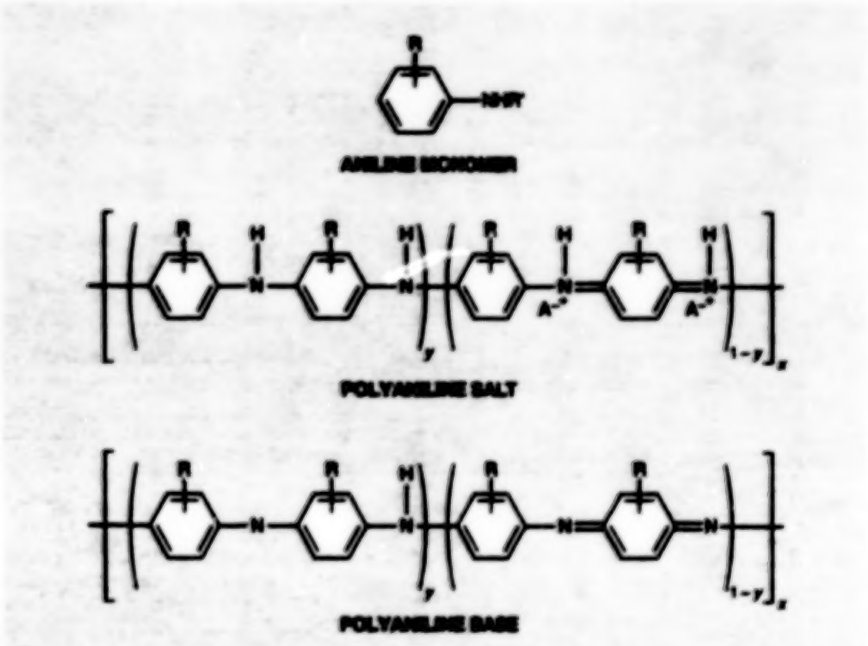

Aniline Monomers and Polymers exist in a variety of molecular structures. "R" and "R'" represent hydrogen and/or alkyl or alkoxyl functional groups containing between 1 and about 6 carbon atoms apiece, "A" represents an anion, and x is an integer. For each polyaniline, y and $1 - y$ ($0 \leq y \leq 1$) denote the proportions of the two types of groups depicted in parentheses; the position of each such group along the molecular backbone is shown for example only and is not known precisely in advance.

Preferably, a coating solution is made from a polyaniline in the base form because of the relatively high solubility of the base form. Solvents that can be used to make polyaniline base solutions include dimethyl sulfoxide, N-methylpyrrolidinone, and tetramethylurea. The concentrations of polyanilines in useful coating solutions lie

approximately in the range between 0.5 and 5 weight percent.

Upon exposure to a corrosive, acidic environment, a polyaniline coating film in base form undergoes a conversion to a doped, electrically conductive salt form. The polyaniline film coating can also be applied to the substrate in a partially doped form; however, the partially doped polyaniline is generally more difficult to dissolve in a given solvent. Useful dopant anionic species that can be used to make partially doped polyaniline coatings include sulfonic acids and camphor sulfonic acid; solvents that can dissolve the resulting partially doped polyanilines include toluene and substituted phenols.

The tenacity of a polyaniline coating can be increased by pretreating the surface of the substrate with a suitable compound. Compounds useful for this purpose are some that simultaneously bind chemically, via covalent or ionic bonds, to the surface of the substrate and to the polyaniline. Among these compounds are phosphoric acid, polyphosphoric acid, and organic chelating agents in which atoms form multiple coordinate bonds with the substrate.

This work was done by N. Ahmad and A. MacDiarmid of the University of Pennsylvania for **Johnson Space Center**. *Further information is contained in a TSP [see page 1].*

In accordance with Public Law 96-517, the contractor has elected to retain title to this invention. Inquiries concerning rights for its commercial use should be addressed to

University of Pennsylvania
Center for Technology Transfer
Suite 300
3700 Market Street
Philadelphia, PA 19104-3147

Refer to MSC-22647, volume and number of this NASA Tech Briefs *issue, and the page number.*

PBO Fiber Blends: A Promise for the Future

At least one blend exhibits superior resistance to abrasion.

Lyndon B. Johnson Space Center, Houston, Texas

Description of Specimen	Tensile Strength Before Abrasion, lb.	Strain, Percent	Energy to Break Point, in.-lb.	Tensile Strength After Abrasion, lb.	Percent Loss of Tensile Strength	LOI, Percent O_2
40 % PBO, 60% Polyimide Hybrid, Plain Weave	3,827	10.57	3,855	1,189	65	51
60 % PBO, 40% Polyimide Hybrid, Plain Weave	4,528	9.25	4,783	1,600	65	56
Pure PBO, Plain Weave, 500 Denier	6,662	11.42	9,216	2,197	67	74
Pure PBO, Double Cloth, 500 Denier	7,880	13.91	12,480	3,880	50.2	75
Aromatic Polyimide, Plain Weave, 1,500 Denier	3,739	8.541	3,772	327.8	91.2	37
PBO/Aramid Felt-PBO (Inside) Aramid Felt Triple Cloth	5,831	6.956	6,002	2,972	47	40

PBO Fiber Blend Test Data shows enhanced abrasion resistance and other similar properties versus PBO alone and polyimide alone.

Woven fabrics comprising polybenzoxazole (PBO) fibers blended with other selected fibers have been found to exhibit combinations of properties that, in some applications, may be superior to those of fabrics made from either PBO alone or the other materials alone. This finding is the result of an investigation of improved fabrics for potential use in space suits and in structures for protecting spacecraft against micrometeoroids. Potential terrestrial applications for the improved fabrics could include bulletproof vests, protective suits for firefighters, and lightweight armor for military equipment and personnel, as well as tethers for parachutes or aircraft.

PBO is characterized by high values of thermo-oxidative stability and tensile strength — a combination of properties that make PBO desirable for many applications, including those described above. However, PBO exhibits some of the same deficiencies — in particular, limited flex life and limited resistance to abrasion — observed in other high-modulus fiber materials. Therefore, woven fiber blends with PBO were investigated in an effort to increase flex life and resistance to abrasion without sacrificing tensile strength or resistance to flames and heat.

In the investigation, enhanced performance was sought through changes in the structures of yarns and fabrics through blending PBO multifilament yarns with other high-performance filamentary materials. Specimens in the form of webs 2 in. (≈5.1 cm) wide were made from PBO and other materials as follows:

- A plied (double-cloth) fabric consisting entirely of PBO (one of two control specimens);
- A plain-weave fabric consisting entirely of PBO;
- A plied fabric consisting entirely of Kevlar aromatic polyamide (the other control specimen);
- A plied yarn hybrid of which 60 percent consisted of PBO fibers and 40 percent consisted of high-temperature-resistant, wear-resistant polyimide fibers known by the trade name "P84";
- A plied yarn hybrid consisting of 40-percent PBO and 60-percent P84 polyimide; and
- A hybrid fabric consisting of 70-percent PBO and 30-percent Nomex aramid felt. The specimens were abraded accord-

ing to a Federal specification for testing for resistance to abrasion. The specimens were tested for tensile strength before and after abrasion. They were also evaluated with respect to limiting oxygen index (LOI) (a measure of resistance to burning).

The table presents some of the data from the tests. The PBO/Nomex-blend specimen resisted abrasion better than did the pure-PBO specimen. Although the LOIs of the blend specimens were less than those of the pure-PBO specimens, they were still much higher than that of any other commercially available polymer fiber fabric of the same density. The LOIs of all samples tested satisfy the flame-resistance requirements for use in the space-shuttle cabin, which is an indication that PBO fiber blends have great potential for spacecraft applications.

This work was done by Evelyne Orndoff of **Johnson Space Center**, *Steven Clarke of Albany International Research Co., and Rajib Dasgupta of Lockheed Martin. Further information is contained in a TSP* *[see page 1]*.

MSC-22957

Electrodeposition of Strong Glassy Metals

Stresses in deposits can be tailored via compositions, temperatures, and current densities.

Marshall Space Flight Center, Alabama

Thin-walled structures made of strong glassy nickel and glassy nickel-cobalt alloys, with tailorable low residual stresses, and with high resistance to permanent plastic deformation, can be formed by use of an electrodeposition process. This process was developed to enable the fabrication of lightweight, high-quality x-ray mirrors that do not undergo unacceptably large distortions when differential thermal contraction upon cooling is used to release the mirror deposits from their electrodeposition mandrels. This process supplants an older pure-nickel electrodeposition process where it was necessary to form relatively thick deposits in order to make them strong enough to resist distortion in the presence of stresses imparted during release.

The process is based on the concept of selecting the composition of a plating bath and controlling the electric-current density to tailor the alloy composition and the level of stress in the electrodeposit. The plating bath contains a mixture of nickel salts, or nickel and cobalt salts with sodium hypophosphite. The bath also contains a surfactant and at least one complexing salt capable of combining with nickel, cobalt, and sodium. The pH of the bath is moderate; consequently, there is little risk of corrosion.

At low temperatures, cobalt contributes to compressive stress, while nickel contributes to tensile stress in the deposit. Thus, by suitable balancing of the ingredients in conjunction with the temperature and current density, it is possible to obtain zero net stress in the deposit throughout any desired thickness. Moreover, for a given suitable formulation of ingredients, the stress can be varied from compressive to tensile by varying the current density at a fixed temperature or by varying the temperature at a fixed current density.

The temperatures used in this process lie in the range from 35 °C, for glassy nickel-cobalt alloys to 70 °C for glassy nickel; as a result, this process is safer than is an electroless process, widely used in airline repair centers, that involves temperatures from 85 to 90 °C. In this process unlike in the electroless process, nickel, and cobalt when used, can be replenished by dissolution from anodes rather than by addition of chemicals. Little effort is required to maintain the plating bath in this process because any occasional chemical adjustments that must be made are much less critical than those needed in the electroless process.

A deposit formed in this process exhibits little or no plastic deformation at the parts-per-million level (microyielding) at stresses below 100 kpsi (0.7 GPa) and has an ultimate strength of greater than 200 kpsi (1.4 GPa). The deposit is also very hard (>50 Rockwell C), permitting diamond tool machining.

This work was done by Brian D. Ramsey of **Marshall Space Flight Center** *and Darell E. Engelhaupt of the University of Alabama in Huntsville. For further information, please contact Darell E. Engelhaupt at (256) 890-6030 or engelhd@email.uah.edu or Sammy Nabors, MSFC Commercialization Assistance Lead, at (256) 544-5226 or sammy.nabors@msfc.nasa.gov.*

In accordance with Public Law 96-517, the contractor has elected to retain title to this invention. Inquiries concerning rights for its commercial use should be addressed to

Darell E. Engelhaupt
Center for Applied Optics
University of Alabama
Huntsville, AL 35899

Refer to MFS-31377, volume and number of this NASA Tech Briefs *issue, and the page number.*

BLANK PAGE

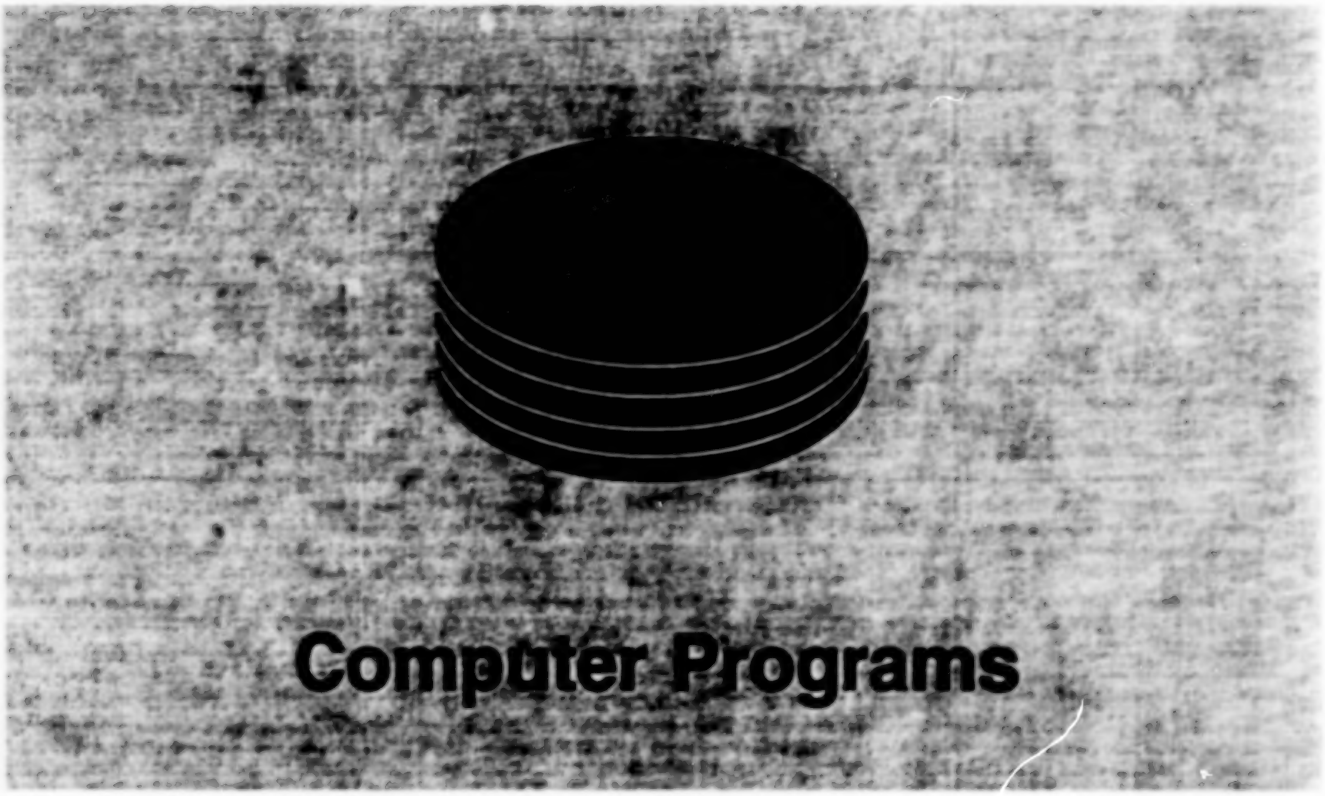

Computer Programs

Electronic Systems

41 Development of a Range-Safety Smart System

Physical Sciences

41 Software for Multidisciplinary Analysis of Optical Systems
41 Program Traces Rays With Quadruple Precision

Materials

42 Software for Multidisciplinary Analysis of Graded Composites

Mechanics

42 Program Predicts Jet Noise
43 Program for Analyzing Static Transmission Error of Helical Gears
43 Software for Acquiring Data on Dynamics of Magnetic Bearings

Mathematics and Information Sciences

43 Program Summarizes Operational Data From a Complex System

BLANK PAGE

Electronic Systems

Development of a Range-Safety Smart System

Range Safety Officers (RSOs) are used by NASA and other government agencies to ensure protection of life and property during launch operations. The current decision-making system used by the RSOs at NASA Wallops Flight Facility (WFF) and the National Ranges, including the Eastern Range (ER) and Western Range (WR), was conceptually developed in the late 1960's and early 1970's. From time to time, improvements have been implemented to increase reliability. However, technology did not exist to make significant improvements in the 3-to-5-second RSO decision-making time. Today, it appears technically feasible to make significant improvements to this system.

Since the 1970's, advances in technology have significantly increased the amount of real-time data, produced low-cost high-speed computer systems, added new data sources, and produced "smart" guidance systems for launch vehicles. Today's telemetry systems provide large quantities of real-time data, which can be readily evaluated by new computer systems. These computer systems now have the processing power and software to perform real-time analyses at low cost, within the decision-making constraints of range safety. Global Positioning Systems (GPSs) have also increased the amount of available decision-making data. Currently, many launch-vehicle systems use smart guidance processors, which compute a new trajectory to orbit once the vehicle has deviated from the pre-launch nominal trajectory. In spite of these advances, the current range safety system does not provide the RSO with the optimum tools to determine whether deviated paths are abnormal vehicle paths or solutions to unexpected conditions.

The Range Safety Smart System (RSSS) was conceived to advance the Range Safety System technology used to make destruct/no-destruct decisions during vehicle flight. The system will provide more accurate and timely advisories on multiple tasks or data inputs within the range safety time constraints of launch vehicle and ground-based systems. A system of processing, analyzing, certifying, and comparing the additional available data, and presenting it to the RSO in a manner which does not add to his/her monitoring burden, will greatly enhance the quality of the real-time destruct/no-destruct decisions; additionally, it will reduce the probability of destructing a good vehicle, increase mission success, and reduce operational cost by reducing the number of RSO support personnel.

In October 1990, Research Triangle Institute (RTI) proposed to utilize computer thought-processing to evaluate real-time RSO decision-making data and present it in a manner that could reduce the RSO's real-time workload and reduce the number of support personnel. In response to this proposal, NASA initiated the RSSS effort. To date, the following have been completed: (1) System Definition, (2) Proof-of-Concept, and (3) Development of a RSSS Demonstration Model. The first two phases were performed by RTI. Phase III, Development of a Demonstration Model, was performed jointly by NASA WFF and RTI.

The demonstration model has been shown to various groups at NASA and DoD. The ER utilized some of the concepts demonstrated in the demonstration model in the Cassini mission. This technology may be adopted by other operational groups at NASA, DoD, and the private sector, who could benefit from its data-acquiring, analyzing, and advising capabilities.

This work was done by Jaya Bajpayee of **Goddard Space Flight Center**. *For inquiries on the RSSS, please contact Jaya Bajpayee at (301)286-0569.*
GSC-13860

Physical Sciences

Software for Multidisciplinary Analysis of Optical Systems

Integrated Modeling of Optical Systems (IMOS) is a MATLAB™ computer program that provides many functions for analysis of a system represented by mathematical models of its thermal, structural, control, and/or optical aspects. For example, IMOS can be used to study thermal distortion of structural components of an optical instrument and the resulting degradation of optical performance. Heretofore, such an analysis would have entailed the use of separate programs to perform thermal, structural, control, and optical sub-analyses. The uniqueness of IMOS lies in the possibility of performing the entire analysis in one program. The common MATLAB™ software environment offers several advantages, including capabilities for optimizing the design of a system on the basis of multidisciplinary (e.g., thermal and optical) criteria and a capability for optimizing the designing of the control subsystem. IMOS provides interfaces between itself and several other programs, including NASTRAN to IMOS, IMOS to SINDA, IMOS to TSS, and IMOS to MACOS. Both MATLAB and IMOS have plotting capabilities that assist in visualization of results.

This program was written by Laura Needels, Hugh Briggs, Andrew Kissil, Daniel Eldred, Marie Levine, James Melody, Mark Milman, Robert Norton, Samuel Sirlin, Miltiadis Papalexandris, Terry Scharton, and Wan Tsoi of Caltech for **NASA's Jet Propulsion Laboratory**. *Further information is contained in a TSP [see page 1].*

This software is available for commercial licensing. Please contact Don Hart of the California Institute of Technology at (818) 393-3425. Refer to NPO-20536.

Program Traces Rays With Quadruple Precision

QRAYPKS is a general-purpose FORTRAN optics-analysis computer program that enables the computation of path lengths to an unprecedented level of precision. The impetus for developing QRAYPKS was the need to mathematically model an outer-space laser interferometer to be used in detecting gravitational waves; the interferometer is expected to have a baseline about 5 million kilometers long, and it is necessary to be able to compute the length of the baseline to subpicometer precision. QRAYPKS can also be used to model other large optical systems in their entirety.

The computer codes used heretofore in designing lenses and other optical systems are capable of single- or double-precision arithmetic and are suitable for modeling of optical systems with dimensions up to a few meters, but double-precision arithmetic cannot, by itself, resolve path lengths to the subpicometer level

over millions of kilometers. In principle, one could obtain the required precision from such a double-precision code by breaking a ray-tracing problem into multiple parts, each small enough that double precision would yield a meaningful result; however, this approach would be time-consuming and susceptible to error.

QRAYPKS is primarily a ray-tracing code: it traces user-specified rays through an optical system that consists of refractive and reflective elements. QRAYPKS can find the intercepts of rays with high-order aspherical surfaces in three dimensions. It can also perform diffraction analysis, approximating a diffraction integral as a sum.

The input to QRAYPKS for specifying an optical system is similar to the input to an optical-design computer program called "CODEV." The main output of QRAYPKS consists of distances along rays between optical surfaces. In addition, because QRAYPKS carries a local coordinate frame with each ray, one can utilize the coordinate frame as part of the basis of a polarization ray-tracing code.

QRAYPKS affords the required path-length precision through the use of quadruple-precision arithmetic. To take advantage of this capability, one must run QRAYPKS on a Digital Alpha (or equivalent) computer, the FORTRAN compiler of which supports quadruple-precision arithmetic. Preferably, the computer should contain integrated circuits capable of performing quadruple-precision arithmetic in hardware, because a software implementation of quadruple-precision arithmetic can multiply the computation time by a factor as large as 100. The machine ε (the smallest increment that, when added to 1, gives a result different from 1) in QRAYPKS is $\approx 10^{-32}$: This level of precision is more than adequate to resolve a subpicometer difference in path length over a multimillion-kilometer baseline.

This program was written by Eugene Waluschka of **Goddard Space Flight Center**. *Further information is contained in a TSP [see page 1].*
GSC-14362

Materials

Software for Multidisciplinary Analysis of Graded Composites

The Coupled Structural/Thermal/Electromagnetic (CSTEM) computer program implements an integrated multidisciplinary approach to analysis and optimization of the designs of graded composite-material structures. The name of the program reflects recognition of the coupling among thermal, electromagnetic, mechanical, and other phenomena in such structures. The integrated multidisciplinary approach is necessary because the coupling among the phenomena gives rise to complexity and contributes to nonlinearity in the characteristics and responses of the structures, such that separate analyses of a structure according to traditionally separate disciplines (e.g., acoustics, structural vibrations, structural loads, thermal effects, and electromagnetic properties taken by themselves) could lead to erroneous conclusions.

CSTEM is written in FORTRAN and is an extended and updated version of the program described in "Multidisciplinary Design of Hot Composite Structures" (LEW-15977), *NASA Tech Briefs*, Vol. 20, No. 3 (March 1996), page 24. As in that program, an essential feature of the multidisciplinary approach is finite-element numerical simulation of the relevant physical phenomena according to the applicable disciplines. The code includes (1) analysis modules that perform calculations pertaining to the separate disciplines and (2) an executive subprogram that controls an iterative solution procedure in which coupling and nonlinearity are taken into account by means of communication of input results among, and coordination of the functions of, the analysis modules. Each analysis module receives the relevant input geometric and control data and transmits any results that may be needed as input for another analysis module.

A notable advanced feature of CSTEM is a capability for analysis of a heterogeneous composite-material structure that contains multiple material layers or other regions, without the necessity of using one element for each layer or region. Such properties as the stiffness, thermal conductivity, and electromagnetic absorptivity of an element that comprises multiple layers or other regions are calculated by use of integration points located at the centroids of the layers or other regions within the element. The composite gradients control the finite-element definition of a structure, with two parameters that can be varied: the number of elements along the gradient and the number of numerical quadrature points within an element.

The structural-analysis module performs a large-deformation analysis, using a unique incrementally updated Lagrangian with iterative refinement. Associated with the large-deformation structural-analysis module is a deformed-position vibration-mode-analysis module. The thermal- and electromagnetic-analysis modules use the same finite elements as does the structural-analysis module; this feature facilitates coupling among the modules.

Some other notable features of CSTEM include the following:

- Capabilities for nonlinear-buckling, transient-heat-transfer, internal-damage (creep, plasticity, fatigue), and acoustical analyses;
- Computation of macroscopic properties of a composite material from the properties of the constituent materials at the microscopic level;
- Computation of electromagnetic absorption of a composite material by use of an easily modifiable database of absorption properties of constituent materials; and
- A capability for generation of internal computational meshes.

This program was written by Christos C. Chamis, Charles A. Farrell, and Bruce N. Canright of **Glenn Research Center** *and Richard L. McKnight, Michael S. Hartle, and Hsin-Tien Huang of General Electric Co. Further information is contained in a TSP [see page 1].*

Inquiries concerning rights for the commercial use of this invention should be addressed to NASA Glenn Research Center, Commercial Technology Office, Attn: Steve Fedor, Mail Stop 4–8, 21000 Brookpark Road, Cleveland, Ohio 44135. Refer to LEW-17052.

Mechanics

Program Predicts Jet Noise

MGBK is a computer program that predicts the mixing noise and the shock noise generated by a subsonic or low-supersonic jet, given input data on the mean flow and turbulence fields as predicted by a suitable state-of-the-art computational fluid dynamics (CFD) program. More specifically, MGBK can be regarded as a post-processing program for use with a CFD program that computes a Reynolds-averaged Navier-Stokes solution with turbulence represented by a mathematical model of a type known in the art as "$k-\varepsilon$" [in which k denotes the time-averaged kinetic-energy density associated with the local fluctuating (turbulent) component of flow, while ε denotes the time-averaged rate of dissipation of this turbulent-kinetic-energy density]. The predictions generated by MGBK are in the forms of sound-pressure levels and frequency spectra on arcs or sidelines.

MGBK is an updated version of a noise-prediction program, called "MGB," devel-

oped during the 1970s. MGBK predicts only the noise generated in the part of a jet plume external to the exit plane of the nozzle of a jet engine; it does not predict mixing or turbomachinery noise generated within the engine. Still, in cases in which external mixing is the dominant cause of noise, MGBK could prove valuable for understanding noise and reducing noise through improvements in the designs of nozzles and/or mixers.

The approach taken in the development of MGB and MGBK has been one of mathematical modeling of noise sources associated with turbulence. In order to predict noise by use of MGBK, one must use an H-type structured computational grid with slices perpendicular to the direction of mean flow. The input to MGBK comprises data on the CFD-predicted flow field on this grid, plus several parameters. Although the prediction of noise applies to the external part of the jet plume only, boundary conditions in CFD predictions are specified well upstream of the nozzle exit and from 20 to 30 diameters downstream of the exit plane.

The input data are processed by means of semiempirical mathematical models of noise-source strength and acoustic propagation. The source model includes both self and shear noise-source terms. Anisotropy of turbulence is incorporated into the source model via an axisymmetric turbulence submodel. Inasmuch as noise is a byproduct of turbulence, the noise predictions of MGBK are unavoidably sensitive to the details of both the CFD input and the noise models and, hence, some degree of empiricism unavoidably enters via the models.

This program was written by Abbas Khavaran of Dynacs Engineering Co. for **Glenn Research Center**. *Further information is contained in a TSP [see page 1].*

Inquiries concerning rights for the commercial use of this invention should be addressed to NASA Glenn Research Center, Commercial Technology Office, Attn: Steve Fedor, Mail Stop 4–8, 21000 Brookpark Road, Cleveland, Ohio 44135. Refer to LEW-17062.

Program for Analyzing Static Transmission Error of Helical Gears

The computer program HeliStat performs finite-element analysis to simulate meshing of helical gears. This program is a logical extension of the program DANST, which applies to spur gears. [DANST was described in "Computing Stresses in Spur Gears (LEW-15420), *NASA Tech Briefs*, Vol. 19, No. 12 (December 1995), page 73 and "Updated Program for Computing Stresses in Spur Gears (LEW-16575) *NASA Tech Briefs*, Vol. 22, No. 8 (August 1998), page 59.]

HeliStat performs a geometric tooth-contact analysis to determine the lines of tooth contact, and then it performs a three-dimensional linear static analysis to determine tooth-meshing stiffness, tooth deflections under static load, and the static transmission error. The results of the static analysis are available to the user in the form of static transmission error as a function of rotation as well as the peak-to-peak transmission error. Since the transmission error is the major source of dynamic excitation that causes gear vibration and noise, HeliStat can help a gear designer develop quiet gears.

The mathematical model upon which HeliStat is based includes representations of the driving and driven gears, connecting shafts, and supporting bearings. The model also includes provisions for gear-tooth modifications either perpendicular to the lines of contact (cross-modification) or in the profile and longitudinal directions. HeliStat can be used for parametric studies of the effects on the transmission error of helical-gear systems due to torque, tooth stiffness, and gear-tooth modifications.

This program was written by H. H. Lin of the University of Memphis and Fred B. Oswald of **Glenn Research Center**.

Inquiries concerning rights for the commercial use of this invention should be addressed to NASA Glenn Research Center, Commercial Technology Office, Attn: Steve Fedor, Mail Stop 4–8, 21000 Brookpark Road, Cleveland, Ohio 44135. Refer to LEW-16877.

Software for Acquiring Data on Dynamics of Magnetic Bearings

A computer program controls the automated acquisition, display, and reduction of data on the dynamics of magnetic bearings. The data gathered by use of this program are expected to enable the verification and enhancement of mathematical models of magnetic-bearing dynamics, thereby contributing to the development of improved magnetic bearings for advanced gas turbine engines and other rotary machines.

With respect to a given magnetic bearing that is part of a rotary machine, the program acquires raw data on rotor position versus time during operation of the machine under known conditions of speed of rotation, temperature, electric currents applied to the electromagnet coils in the bearing, and shaking. The program processes the raw data to characterize the bearing with respect to dynamic position stiffness, current stiffness, and damping coefficients versus speed of rotation, eccentricity, bias current, temperature, and frequency of shaking. The program can also account for friction, stiffnesses of structural supports, inertia, and uncertainties.

The program was developed by use of the LabVIEW software system and the corresponding NI-DAQ programming language. The program provides the user with four major options called "16 Time," "16 Frequency," "Stiffness," and "Alignment." The first two options enable the monitoring of 16 analog input channels to obtain time- and frequency-domain responses. These options also enable the generation of four orbit displays and provide for the recording, in a text file, of the magnitudes and phases of the components of motion at the shaking frequency. The Stiffness option provides for the measurement and recording of the position and the current stiffness of the magnetic bearing, using data from 14 input channels. The stiffness option also includes a provision for calculating uncertainties. The Alignment option generates a graphical display of stator alignment with a bar chart of eight dynamic load cells.

This program was written by Gerald Montague and Al Kascak of the U.S. Army Research Laboratory and Alan Palazzolo of Texas A&M University for **Glenn Research Center**. *Further information is contained in a TSP [see page 1].*

Inquiries concerning rights for the commercial use of this invention should be addressed to NASA Glenn Research Center, Commercial Technology Office, Attn: Steve Fedor, Mail Stop 4–8, 21000 Brookpark Road, Cleveland, Ohio 44135. Refer to LEW-17057.

Mathematics and Information Sciences

Program Summarizes Operational Data From a Complex System

Engineering Data Summarization Flight Software is a computer program designed for use aboard a spacecraft to implement a concept, called "beacon monitoring," that has been discussed in several prior *NASA Tech Briefs* articles. The program generates summaries of operational data (e.g., sensor readings) that represent the

state of the spacecraft, and thereby reduces both (1) the quantity of information that must be telemetered to a ground station and (2) the time and cost of analyzing the data to diagnose the spacecraft. The program can also be used to reduce the cost of diagnosing a complex terrestrial system. The program generates event-driven summaries of events since the last contact. For each event, the program identifies the sensor and its readout data that triggered increased monitoring, and gathers data from that sensor and causally related sensors at a high sampling rate around the time of the event. The data from all such events are assigned priorities and stored for downlink at the next telemetry pass. Gaps in the data between events are filled by "snapshots" of all sensor channels sampled at a lower rate. Triggering for each event can be effected by use of either static alarm thresholds or adaptive thresholds established by artificial-intelligence subprograms.

This program was written by E. Jay Wyatt, Dennis Decoste, Alan Schlutsmeyer, Robert Sherwood, and John Szijjarto of Caltech for **NASA's Jet Propulsion Laboratory**. *Further information is contained in a TSP [see page 1].*

This software is available for commercial licensing. Please contact Don Hart of the California Institute of Technology at (818) 393-3425. Refer to NPO-20822.

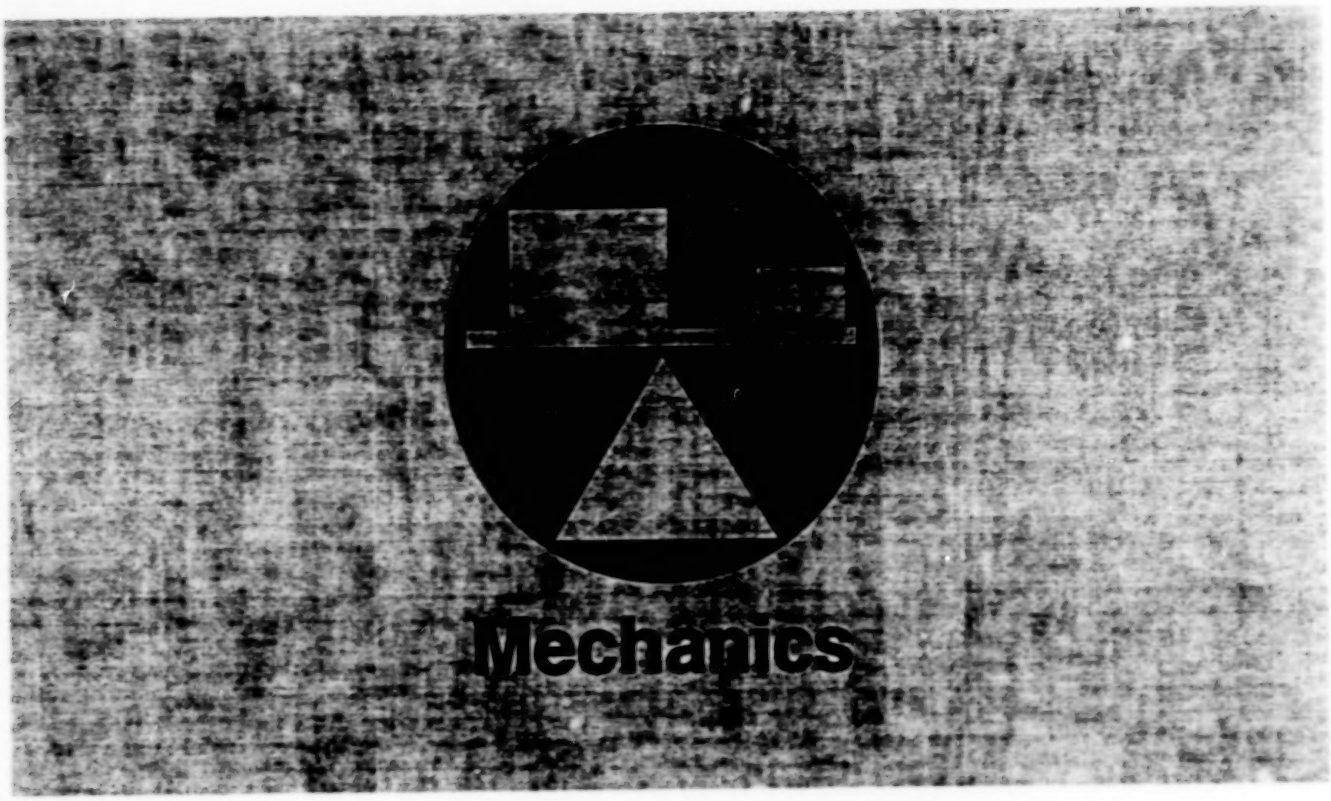

Hardware, Techniques, and Processes

47 Air-Displacement Volumometer With Soft Sides
47 Improved Methodology for Dynamics of Orbiter Payload Bay Doors

4/6

BLANK PAGE

Air-Displacement Volumometer With Soft Sides

Complete submersion of the subject in water is no longer necessary.

Lyndon B. Johnson Space Center, Houston, Texas

An air-displacement volumometer with soft sides has been devised for measuring the volume of a human body. This apparatus could be useful in hospitals, medical research laboratories, clinics, athletic facilities, and the like. It could also be used to measure the volumes of irregularly shaped objects with dimensions comparable to those of a human body.

The traditional procedure for measuring the volume of a human body is based on the Archimedean principle of weighing the subject in air, then weighing the subject underwater, then equating the volume of the subject to the volume of water displaced, as indicated by the difference between the two weight measurements. In this procedure, the subject is required to exhale totally, hold his or her breath, and submerge totally in water. The traditional procedure is obviously not suitable for subjects who are hydrophobic or averse to total exhalation.

The use of air-displacement volumometers does not involve immersion, and total exhalation is unnecessary. Air-displacement volumometers with hard sides were used during the early 1960s, but were abandoned because they gave relatively inaccurate results (±5 percent). Moreover, hard-sided air-displacement volumometers were large and not portable. The present soft-sided air-displacement volumometer gives relatively accurate results (±0.15 percent) and is portable.

The soft-sided air-displacement volumometer consists mostly of a hermetic bag with pressure ports and a hermetically sealing zipper (see figure). The bag is also marked with two compression stops; these are lines to which the lower end of the bag is rolled to provide compression to a sequence of known volumes. The measurement procedure is as follows:

1. The subject enters the bag, which is then zippered shut.
2. The bag is inflated to a gauge pressure of 10 cm H_2O (0.98 kPa).
3. The subject is asked to hold his or her breath during the next step.
4. The bag is rolled up to the first compression stop and held there momentarily, then rolled up to the second compression stop. The pressure is recorded continuously during this compression process.
5. The subject is instructed to breathe.
6. Steps 2 through 5 are repeated four more times to obtain a total of five trials, each involving a sequence of three pressure measurements (the initial inflation pressure and the pressures at the two compression stops).

Using the ideal-gas law, one calculates the volume of the person or irregular object in the bag from the nominal empty-bag volumes and corresponding pressure readings at initial inflation and the two compression stops for each trial. The calculated volumes are then averaged over the five trials. The results of these calculations are independent of the elasticity of the bag, provided that the elasticity of the bag remains constant over the small ranges of pressure and volumes used in the measurements.

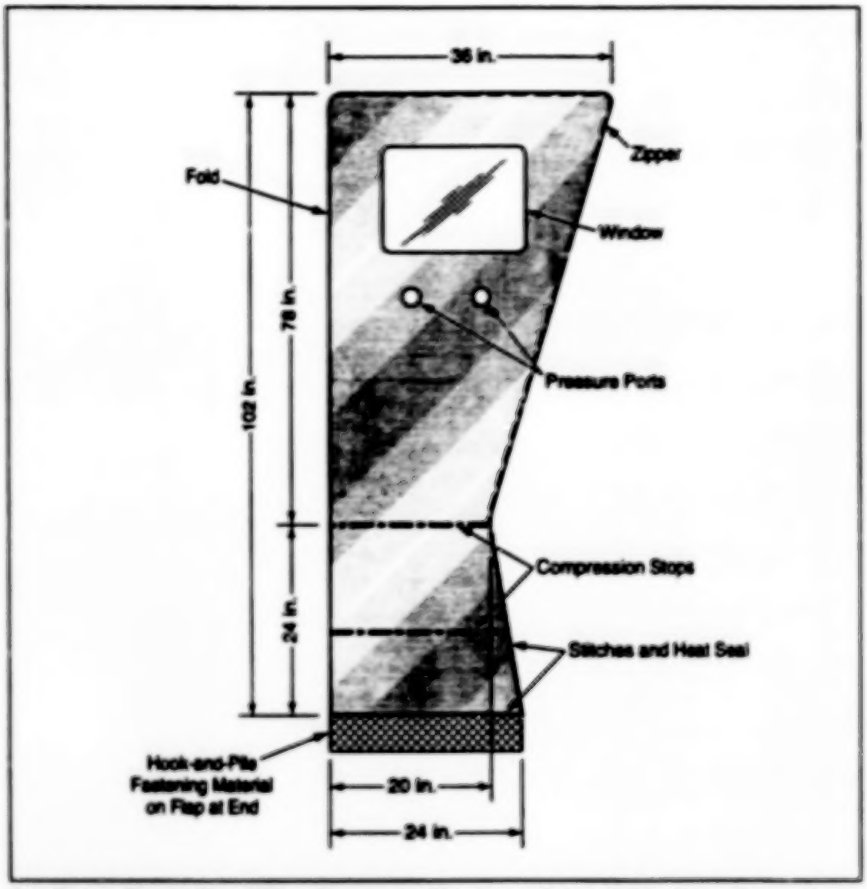

The Bag Is Zipped Shut With a Person Inside, then inflated slightly, then rolled up to the compression stops in sequence, all the while recording the pressure in the bag. The volume of the person can be computed from the pressure readings and the nominal (zero-pressure) empty-bag volumes.

This work was done by Steven F. Siconolfi of **Johnson Space Center.** *Further information is contained in a TSP [see page 1].*

This invention has been patented by NASA (U.S. Patent No. 5,948,977). Inquiries concerning nonexclusive or exclusive license for its commercial development should be addressed to the Patent Counsel, Johnson Space Center, (281) 483-0837. Refer to MSC-22653.

Improved Methodology for Dynamics of Orbiter Payload Bay Doors

The Payload Bay Door Dynamics Simulation (PBDS) computer program simulates the mechanical behavior of the space-shuttle payload bay doors and their latching and driving mechanisms during opening, closing, latching, and unlatching. PBDS was developed to replace an older program that was computationally inefficient and that simulated the door hinges incorrectly. In PBDS, the large system of dynamical equations of the payload-bay-door system is decomposed into smaller

systems of dynamical equations at the mechanism level. This decomposition involves decoupling through neglect of the inertial parameters of the driving and latching mechanisms, which are small relative to those of the doors. The equations of motion of the doors, which are flexible, are derived by use of a Cartesian flexible-body formulation. The equations of motion of the mechanisms are derived by use of an efficient recursive formulation. Though decoupled dynamically, the door and the mechanisms are coupled kinematically. In solving the mechanism equations, the responses of the door at points where the door is attached to the mechanisms are fed as inputs to the mechanism equations. The outputs of the mechanism equations are forces and torques, which are fed back to the door equations to complete the computational cycle.

This work was done by Shih-Chin Wu of Boeing North American, Inc., for **Johnson Space Center**. *Further information is contained in a TSP [see page 1].*
MSC-22845

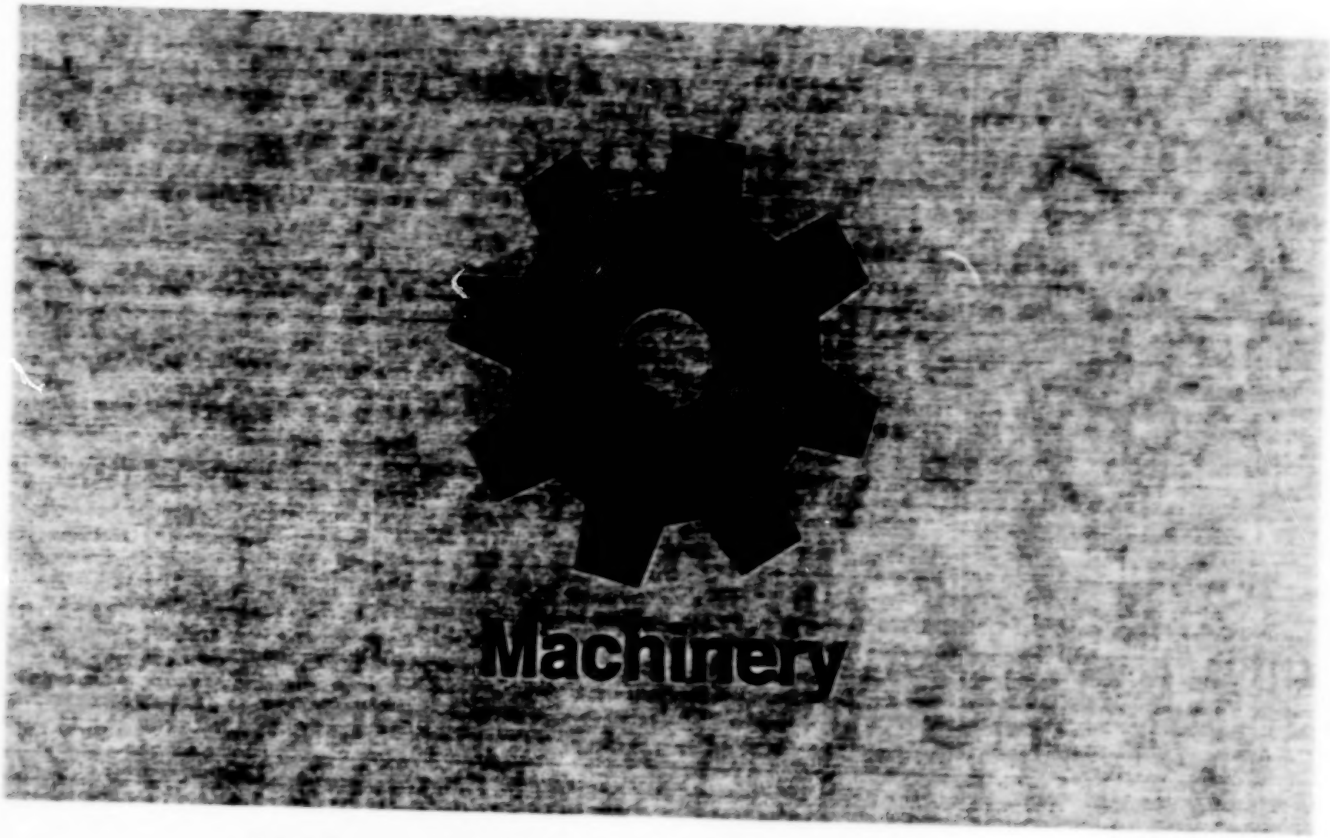

Hardware, Techniques, and Processes

51 Computer-Controlled Power Tool
52 Technique for Controlling Gas Generation in a Bioreactor

BLANK PAGE

Computer-Controlled Power Tool

Torque or speed is regulated, and operational history can be analyzed.

Goddard Space Flight Center, Greenbelt, Maryland

The figure depicts the exterior appearance of a pistol-grip rotary power tool that can be used to turn a drill bit, wrench socket, screwdriver, or other tool bit clockwise or counterclockwise at a controlled speed or torque. This tool is an updated version of the one described in "Pistol-Grip Torques-Measuring Power Tool" (GSC-13706), *NASA Tech Briefs*, Vol. 23, No. 7 (July 1999), page 36. Like other tools that it superficially resembles, it contains an electric motor drive powered by either a battery or a power-supply circuit with a standard power-line connection. Unlike other such tools, this tool also contains the following:

- Torque and temperature sensors;
- Shaft-rotation pulse-counting and timing circuitry for measuring speed;
- External controls for setting the mode of operation, the direction of rotation, and the desired value of speed or torque;
- An onboard computer that generates its own timing signals and monitors and controls the overall operation of the tool;
- A drive circuit through which the onboard computer controls the electric current applied to the motor;
- An alphanumeric display for use in programming and monitoring operational parameters;
- Light-emitting-diode (LED) torque, power-on/off, and fault indicators; and
- A port for communication between the onboard computer and an external computer.

In the customary manner, the operator of the tool presses a trigger to put the tool in a running state and releases the trigger to put the tool in an idling state. During operation, the digital outputs of the torque and temperature sensors and of the speed-measuring circuitry are presented to the onboard computer. The software in the onboard computer implements an interrupt-driven state machine for the purposes of monitoring operational parameters, controlling speed or torque, keeping a history of operation, and communicating with the external computer.

The history of operation includes records of two types: (1) data on torque and shaft angle as functions of time during the tightening and/or loosening of fasteners; and (2) records of events (e.g., turn-on of power or overheating). These records are stored in nonvolatile memories in the onboard computer. The onboard and external computers communicate with each other for the purpose of transferring these records so that the external computer can be used to analyze operation and/or to modify operational parameters. Operational parameters can be transferred from the external computer to a nonvolatile memory in the onboard computer; thus, in effect, the external computer can program and remotely control the tool.

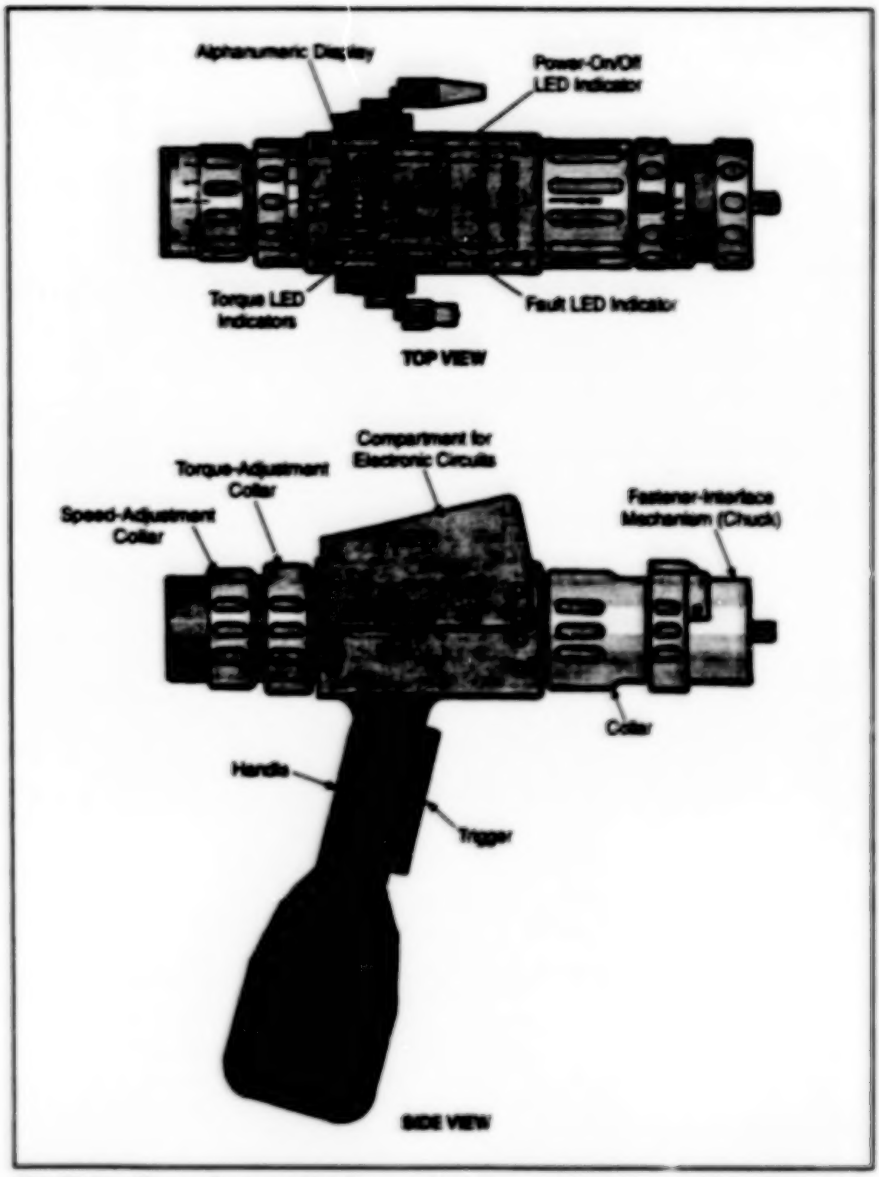

This Rotary Power Tool superficially resembles other such tools but includes additional circuitry, including an onboard computer, that provides enhanced capabilities for control of speed and torque, detection of faults, and analysis of operation.

This work was done by Kenneth W. Wagner, James C. Taylor, and Paul W. Richards of **Goddard Space Flight Center**. *Further information is contained in a TSP [see page 1].*

This invention has been patented by NASA (U.S. Patent No. 5,903,462). Inquiries concerning nonexclusive or exclusive license for its commercial development should be addressed to the Patent Counsel, Goddard Space Flight Center [see page 1]. Refer to GSC-13879.

Technique for Controlling Gas Generation in a Bioreactor

In the reactor, bubbles are suppressed by pressurizing the liquid flowing through it.

Lyndon B. Johnson Space Center, Houston, Texas

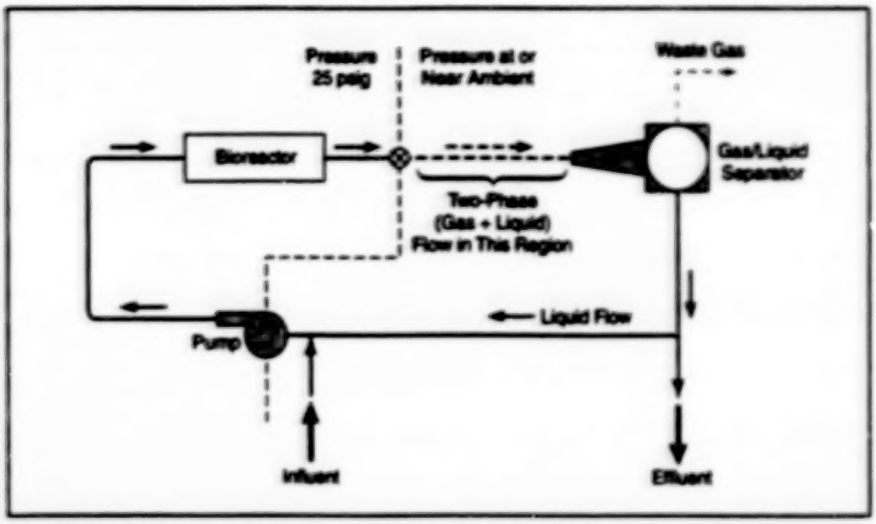

The Higher Pressure in the portion of the flow path that includes the bioreactor keeps gases in solution. The lower pressure in the portion of the flow path that includes the gas/liquid separator allows gases to come out of solution.

A pressure-swing technique has been developed for controlling the generation and flow of gas in an anaerobic biological reactor and associated equipment in a system that processes wastewater. The purpose and effect of the technique is to prevent the formation of gas bubbles in the reactor; if allowed to coalesce in the reactor, gas bubbles could impede the flow of the liquid stream, rendering the treatment system less effective. The technique was conceived for application to a wastewater treatment system that would operate in microgravity, but could also be applied to bioreactor systems (e.g., fermentation systems) that operate in Earth-normal gravity.

A representative system that implements the present technique (see figure) includes a packed-bed reactor that is inoculated with anaerobic micro-organisms, a gas/liquid separator, a pump, a back-pressure relief valve, and associated plumbing and other hardware. Wastewater is fed into the system at a constant rate, and effluent is removed from the system at the same rate, both at a pressure near ambient. The pump pressurizes the water to 25 psig (gauge pressure of 172 kPa) and circulates the water through the bioreactor at a rate of 20 times the influent/effluent rate. After passing through the reactor, the water flows through the back-pressure relief valve and is thereby depressurized to near ambient pressure.

In the reactor, the pressure is high enough to keep all gases in solution; this includes gaseous waste products generated by micro-organisms through their metabolism of contaminants in the wastewater. The depressurization causes the gaseous waste products generated in the reactor to evolve into gas bubbles. The resulting two-phase mixture flows into a gas/liquid separator. The separated gases are vented to the atmosphere, and the separated liquid travels to the pump, where it is repressurized for the next pass through the reactor.

The design size of the reactor is based on the desired rate of flow and the anticipated daily contaminant loading of the wastewater to be treated. The reactor pressure and the ratio between the recirculating flow and the inlet or outlet flow could differ from the values stated above; for a given application, they are calculated to maintain gases in solution in the bioreactor. In general, the use of a higher pressure makes it possible to reduce the liquid recirculation rate.

This work was done by Karen D. Pickering and Eugene K. Unger of **Johnson Space Center**. *Further information is contained in a TSP [see page 1].*

MSC-22987

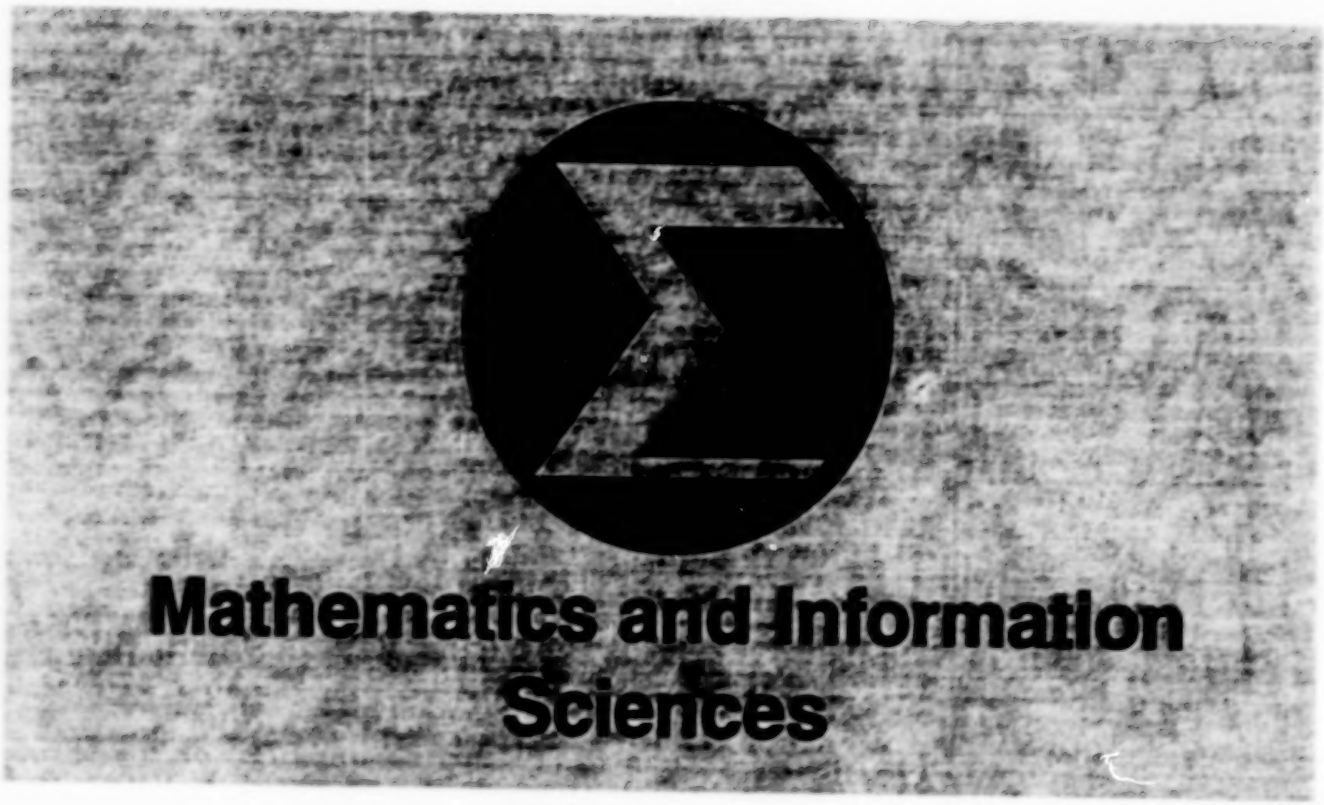

Mathematics and Information Sciences

Hardware, Techniques, and Processes

55 Linking Employee Apporaisals to Organizational Goals
56 Neural-Network Approach to Analysis of Sensor Data
57 Program for Visualization and Exploration of Scientific Data

BLANK PAGE

Linking Employee Appraisals to Organizational Goals

Evaluation of employee performance would be systematized, centralized, and automated.

John F. Kennedy Space Center, Florida

The GPES Home Page and a standard form for editing employee data are two examples of interactive displays provided by the GPES via the Internet, for use by employees and managers.

The Goal Performance Evaluation System (GPES) is an Internet-based automated management information system (see figure) now undergoing development at Kennedy Space Center (KSC). The GPES is designed to perform two major functions:

1. Serve as a strategic management tool that directly links through automation the goals and objectives of the NASA Strategic Plan and KSC Implementation Plan through individual performance plans; and
2. Serve as a Performance Management tool that facilitates the definition, appraisal, and strategic linking of every civil service employee performance plan to the NASA Strategic Plan.

According to NASA's Strategic Management Handbook, the final linkage between each employee's performance and high-level organizational goals is made via the employee's performance plan and appraisal, but heretofore, linkage processes had not been defined by NASA or by KSC. The GPES would define the linkage processes and would serve as a central, systematic, automated means to implement the processes. The GPES consists of two parts: (1) the Integrated Business System Model (IBSM) and (2) a data-base application program.

The IBSM defines the documents and processes for relating NASA and KSC goals to the employee. The IBSM is an updated means of administering three management systems that have been in use at KSC: ISO-9000, Strategic Planning, and the Employee Performance Communication System (EPCS). The IBSM was developed to reduce the work of maintaining these systems and to improve understanding of interrelationships among them.

The data-base application program makes it possible to maintain all 1,700 employees' performance plans in one central data base. Some features of the program are the following:

- A manager adds items to an employee's performance plan by selecting them from a pull-down list of objectives and strategies.
- An employee can provide information on major accomplishments relevant to items in his or her performance plan. Additionally, the system facilitates the assimilation of employee/manager achievement data into office, directorate, and Center-wide reports.
- A manager can review information provided by an employee and add performance-assessment comments.
- The employee's performance plan can be printed on the KSC standard EPCS form.
- The program generates several reports, including one that shows a distribution of the number of employees contributing to each strategy.
- Performance plans for the entire Center can be changed simultaneously to reflect redirection in Agency/KSC Strategic Plans, or rephrasing of current objectives and strategies. Heretofore, each employee's performance plan was stated in a separate document, maintained by use of word processing software, that a manager or secretary had to update individually.

At the time of reporting the information for this article, the Internet application program has successfully completed its first performance development cycle both at KSC and at the Johnson Space Center. Based on the organizational and management benefits, Stennis Space Center is currently deploying the Internet application for the 1999 – 2000 year performance cycle. In addition, the Marshall Space Flight Center and the Langley Research Center are both evaluating the application as a pilot program.

Anticipated organizational benefits from the GPES, in addition to those mentioned above, include the following:

- Closer alignment between resources and high-level organizational goals;
- Increase in efficiency through automation and standardization of performance planning;
- Encouragement of cross-functional job assignments for employees through the on-line performance definition and assessment from multiple supervisors;
- Increase in communication;
- More feedback for better monitoring of how well the organization and its subdivisions are performing; and
- Facilitation of changes in organizational roles.

This work was done by Christopher J. Carlson, Jennifer C. Kunz, and Lesa B. Roe of **Kennedy Space Center**. *Further information is contained in a TSP [see page 1].*

Inquiries concerning rights for the commercial use of this invention should be addressed to the Technology Programs and Commercialization Office, Kennedy Space Center, (407) 867-6373. Refer to KSC-12036.

Neural-Network Approach to Analysis of Sensor Data

Anomalies in dynamic systems are detected by processing seemingly random time series.

NASA's Jet Propulsion Laboratory, Pasadena, California

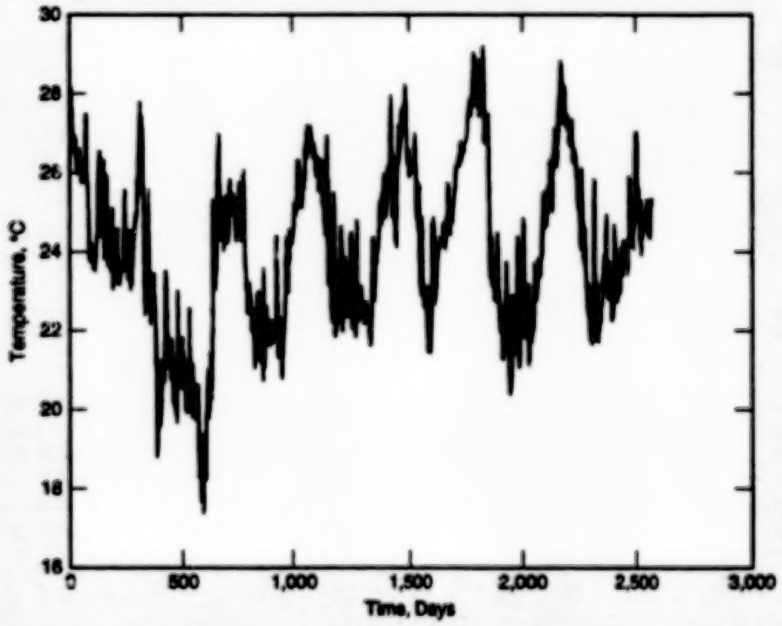

Daily Measurements of Sea-Surface Temperature collected for 2,573 days (slightly more than 7 years) were used in a test of the method.

A method of processing of time-series data from sensors that monitor a dynamic physical system has been devised to enable detection of anomalies in the dynamics. The method involves computing what are initially supposed to be dynamical invariants that represent the structural and operational parameters of the system; the invariants are specified in such a way that anomalies or abnormalities in the system manifest themselves as changes in the supposed invariants. The method could be applied, for example, to telemetric data from a spacecraft or to such time-series scientific data as sea-surface temperatures measured at daily or other regular intervals.

Abnormal behavior of the system can be detected by (1) predicting the future time series from current and previous time-series values, then (2) recording the actual time series going forward from the instant of prediction, then (3) suitably analyzing the differences between the predicted and recorded values. For the purpose of the present method, it is assumed that the invariants of the system can be represented by the coefficients of a differential or time-delay equation that represents the dynamics of the system.

An important element of the mathematical basis of the method is the concept that there are two types of abnormal behavior of a dynamic system: structural and operational. Structural abnormalities are caused by changes in the underlying dynamics and thus manifest themselves mathematically as changes in the supposed invariants. Operational abnormalities can be caused by unexpected changes in initial conditions or in external forces, but the dynamical model of the system remains the same. Mathematically, operational abnormalities

are described by changes in nonstationary components of the time series. Structural and operational abnormalities can occur independently of each other.

The major problems addressed by the method are how to build a dynamical model that simulates a given time series and how to develop the dynamical invariants, changes of which indicate structural abnormalities. Because the solutions of these problems are so multifaceted and complex that a description of them would greatly exceed the space available for this article, it must suffice to summarize them as follows: The solutions are based on progress in three independent fields — nonlinear dynamics, theory of stochastic processes, and artificial neural networks. One especially notable aspect of the method is that the dynamical model of a system is fitted to the previous and present time-series data by use of a feedfoward neural network that contains only one hidden layer. This technique of fitting is justified by a rigorous proof that any continuous function can be approximated by such a neural network.

The method has been tested by applying it to daily readings of sea-surface temperature collected by an instrumented buoy from May 1987 through May 1994 (see figure). The purpose of the test was to demonstrate that anomalies in the temperature dynamics could be found by use of the present method. Using knowledge of when El Niño and La Niña occurred, an attempt was made to show that the anomalies found by the present method correspond to these phenomena in some manner. An attempt was also made to formulate a way of using the method to predict El Niño and La Niña. At the time of reporting the information for this article, no conclusions concerning the efficacy of the method had been drawn, and there appeared to be a need for more experiments.

This work was done by Sandeep Gulati and Michail Zak of Caltech for **NASA's Jet Propulsion Laboratory**. *Further information is contained in a TSP [see page 1].*

In accordance with Public Law 96-517, the contractor has elected to retain title to this invention. Inquiries concerning rights for its commercial use should be addressed to

Technology Reporting Office
JPL
Mail Stop 249-103
4800 Oak Grove Drive
Pasadena, CA 91109
(818) 354-2240

Refer to NPO-20834, volume and number of this NASA Tech Briefs issue, and the page number.

Program for Visualization and Exploration of Scientific Data

WebWinds is an interactive computer program that aids the visualization and exploration of scientific data. WebWinds is the successor to LinkWinds, which was reported in "LinkWinds — Flexible Software for Highly Interactive Visual Data Analysis" (NPO-19786), *NASA Tech Briefs*, Vol. 20, No. 12 (December 1996), page 46. WebWinds is a platform-independent, reusable code written in the Java computer language. WebWinds has been tested on Linux, Sun, SGI, and Win95 systems.

This program was written by Martin Orton, Lee Elson, Jeff Goldsmith, and William Weibel of Caltech for **NASA's Jet Propulsion Laboratory**. *Further information is contained in a TSP [see page 1].*

This software is available for commercial licensing. Please contact Don Hart of the California Institute of Technology at (818) 393-3425. Refer to NPO-20685.

END

12-4-01